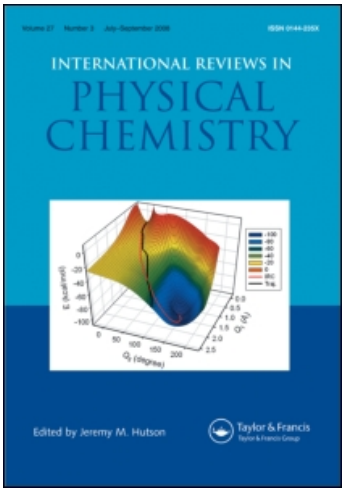

International Reviews in Physical Chemistry
Publication details, including instructions for authors and subscription information:
http://www.informaworld.com/smpp/title~content=t713724383

Bohr model and dimensional scaling analysis of atoms and molecules

Anatoly Svidzinsky[ab]; Goong Chen[c]; Siu Chin[a]; Moochan Kim[ab]; Dongxia Ma[a]; Robert Murawski[ab]; Alexei Sergeev[ab]; Marlan Scully[ab]; Dudley Herschbach[d]
[a] Institute for Quantum Studies and Department of Physics, Texas A & M University, College Station, TX 77843 [b] Applied Physics and Materials Science Group, Engineering Quad, Princeton University, Princeton 08544 [c] Institute for Quantum Studies and Department of Mathematics, Texas A & M University, College Station, TX 77843 [d] Institute for Quantum Studies and Department of Chemistry, Texas A & M University, College Station, TX 77843

To cite this Article Svidzinsky, Anatoly , Chen, Goong , Chin, Siu , Kim, Moochan , Ma, Dongxia , Murawski, Robert , Sergeev, Alexei , Scully, Marlan and Herschbach, Dudley(2008) 'Bohr model and dimensional scaling analysis of atoms and molecules', International Reviews in Physical Chemistry, 27: 4, 665 — 723
To link to this Article: DOI: 10.1080/01442350802364664
URL: http://dx.doi.org/10.1080/01442350802364664

International Reviews in Physical Chemistry
Vol. 27, No. 4, October–December 2008, 665–723

Taylor & Francis
Taylor & Francis Group

Bohr model and dimensional scaling analysis of atoms and molecules

Anatoly Svidzinsky[ac], Goong Chen[b], Siu Chin[a], Moochan Kim[ac], Dongxia Ma[a]*, Robert Murawski[ac], Alexei Sergeev[ac], Marlan Scully[ac] and Dudley Herschbach[d]

[a]*Institute for Quantum Studies and Department of Physics, Texas A & M University, College Station, TX 77843;* [b]*Institute for Quantum Studies and Department of Mathematics, Texas A & M University, College Station, TX 77843;* [c]*Applied Physics and Materials Science Group, Engineering Quad, Princeton University, Princeton 08544;* [d]*Institute for Quantum Studies and Department of Chemistry, Texas A & M University, College Station, TX 77843*

(*Received 17 June 2008; final version received 21 July 2008*)

It is generally believed that the old quantum theory, as presented by Niels Bohr in 1913, fails when applied to few electron systems, such as the H_2 molecule. Here we review recent developments of the Bohr model that connect it with dimensional scaling procedures adapted from quantum chromodynamics. This approach treats electrons as point particles whose positions are determined by optimizing an algebraic energy function derived from the large-dimension limit of the Schrödinger equation. The calculations required are simple yet yield useful accuracy for molecular potential curves and bring out appealing heuristic aspects. We first examine the ground electronic states of H_2, HeH, He_2, LiH, BeH and Li_2. Even a rudimentary Bohr model, employing interpolation between large and small internuclear distances, gives good agreement with potential curves obtained from conventional quantum mechanics. An amended Bohr version, augmented by constraints derived from Heitler–London or Hund–Mulliken results, dispenses with interpolation and gives substantial improvement for H_2 and H_3. The relation to *D*-scaling is emphasized. A key factor is the angular dependence of the Jacobian volume element, which competes with interelectron repulsion. Another version, incorporating principal quantum numbers in the *D*-scaling transformation, extends the Bohr model to excited *S* states of multielectron atoms. We also discuss kindred Bohr-style applications of *D*-scaling to the H atom subjected to superstrong magnetic fields or to atomic anions subjected to high frequency, superintense laser fields. In conclusion, we note correspondences to the prequantum bonding models of Lewis and Langmuir and to the later resonance theory of Pauling, and discuss prospects for joining *D*-scaling with other methods to extend its utility and scope.

Keywords: Bohr model; dimensional scaling; chemistry bond; molecules; potential curves

Contents

*Corresponding author. Email: dma@physics.tamu.edu

ISSN 0144–235X print/ISSN 1366–591X online

DOI: 10.1080/01442350802364664
http://www.informaworld.com

1. Introduction

Quantum chemistry has achieved excellent agreement between theory and experiment, even for relatively large molecules, by using computational power to overcome the difficulty of treating electron–electron interactions [1–11]. The usual discussions of molecular electronic structure are based on solving the many-particle Schrödinger equation with varying degrees of sophistication. These include diffusion Monte Carlo methods [12], coupled cluster expansions, configuration interaction, density functional theory [2], and reduced density matrix mechanics [13]. All are intensely computational and a physically appealing picture of the chemical bond is left behind. Despite the successful tools of modern computational chemistry, there remains a need for understanding electronic structures in some relatively simple way that is capable of describing ground and excited states of atoms and molecules with useful accuracy.

In this review we bring together recent work which resurrects the venerable Bohr model, showing its utility for treating multielectron atoms and molecules. Beyond intuitive, pedagogic appeal, the model is found to yield molecular potential energy curves with surprisingly good accuracy. The new appreciation of the Bohr model has emerged from a dimensional scaling (D-scaling) approach to electronic structure [14]. This unconventional procedure emulates a method developed for quantum chromodynamics [15].

By generalizing the Schrödinger equation to D dimensions, introducing a D-dependent length scale, and passing to the large-D limit, quantum dynamics morphs into classical mechanics. That has provided a congenial link between prequantum and postquantum descriptions of atomic structure and the chemical bond, reconciling Bohr and Sommerfeld with Heisenberg and Schrödinger.

Taking the dimension of space as a variable has become a customary expedient in statistical mechanics, in particle and nuclear physics, and in quantum optics. Typically a problem is solved for some 'unphysical' dimension $D \neq 3$ where the physics becomes much simpler, and perturbation theory is employed to obtain an approximate solution for $D = 3$. A celebrated instance of this strategy was Wilson's use of exact values attained at $D = 4$ to obtain accurate critical exponents for $D = 3$ phase transitions, thereby solving a wide class of notoriously recalcitrant problems of long-standing [16,17].

Impetus for much work pursuing dimensional scaling stratagems in chemical physics, antecedent to that reviewed here, came from a tutorial article published in 1980 by Witten [15]. In discussing quarks, gluons, and 'impossible problems' of quantum chromodynamics, he emphasized an aspect shared with atomic physics. Often physical parameters, such as masses and charges of particles, 'disappear' from dynamical equations when variables such as distances and energies are expressed in terms of dimensionless ratios. In that case, there is no 'free parameter' that can be used to set up a perturbation or interpolation calculation. Then a quantity like dimension, that otherwise would be considered as given and fixed, may be treated as variable, in order to provide a perturbation parameter.

Witten illustrated the procedure with a rough calculation of the large-D limit for the ground states of hydrogen and helium atoms. His results differed from $D = 3$ by $\sim$60%, and he concluded that the method looked unpromising for electronic structure. However, simple improvements were found to markedly reduce the error. Merely using the exact D-dependence for the H atom to define D-scaled distance and energy units sufficed to bring the large-D limit for He within $\sim$5% of the $D = 3$ result. Furthermore, the accuracy for He was improved to 5 significant figures by interpolation between the $D \to \infty$ and $D \to 1$ limits [18] and to 9 figures by a perturbation expansion in $1/D$ [19,20]. Other prototype applications of D-scaling, compiled in two books [14,21] and several review articles [22–28], confirmed its utility for treating non-separable problems involving strong dynamical interactions.

Among aspects of D-scaling of electronic structure that need further study are procedures for molecules and for excited atomic states. The hydrogenic D-scaling, which works well for ground state atoms, when applied to the H_2^+ molecule fails to give chemical bonding at the large-D limit. This occurs because the length scale for the internuclear distance is independent of that for the electrons, so a different scaling scheme (termed 'uniform') is required. Likewise, use of hydrogenic scaling caused excited atomic states to collapse to the ground state in the large-D limit. Among the welcome virtues of the work reviewed here is that both these shortcomings are overcome in the renascent Bohr model.

2. Bohr model as a large-D limit of wave mechanics

Niels Bohr, in July, 1912, at the end of his three month postdoctoral visit to Manchester, sent an outline of his ideas 'On the constitution of atoms and molecules' to his mentor, Ernest Rutherford. In analysing models having Rutherford's point-like nuclei, Bohr

emphasized that 'There seems to be nothing to allow us from mechanical considerations to discriminate between different radii and times of vibration [of electron motions].' Thus, convinced that classical physics cannot explain the atom, Bohr was provoked to 'introduce . . . a hypothesis, from which we can determine the quantities in question'. That led Bohr to the results presented in his celebrated trilogy of 1913 papers [29–31]. In accord with his concern about a length scale, we now find that introducing a D-dependent length scale converts the large-D limit of the Schrödinger equation into Bohr's model.

In contrast to the uncanny success of the Bohr model for a one-electron atom, efforts to apply it to the H_2 molecule or larger systems proved unsatisfactory [32,33]. However, with modest extensions, we find the model does provide surprising accuracy for potential energy curves of H_2 and other molecules and a new perspective on configurations of multielectron atoms.

2.1. *Derivation of the Bohr model for H_2 via D-scaling*

We first outline the variant of D-scaling recently applied to H_2 [34] and then indicate how it differs from what preceded [14,35]. Figure 1 displays coordinates specifying electronic positions in the H_2 molecule. All distances are expressed in terms of the Bohr length $a_0 = \hbar^2/me^2$, where m is the electron mass and e its charge, and energies are in the Hartree unit e^2/a_0. We start with the Schrödinger equation $\hat{H}\Psi = E\Psi$; for H_2, the Hamiltonian is:

$$\hat{H} = -\frac{1}{2}\nabla_1^2 - \frac{1}{2}\nabla_2^2 + V(\rho_1, \rho_2, z_1, z_2, \phi). \tag{2.1}$$

The Coulomb potential energy V is given by

$$V = -\frac{Z}{r_{a1}} - \frac{Z}{r_{b1}} - \frac{Z}{r_{a2}} - \frac{Z}{r_{b2}} + \frac{1}{r_{12}} + \frac{Z^2}{R}, \tag{2.2}$$

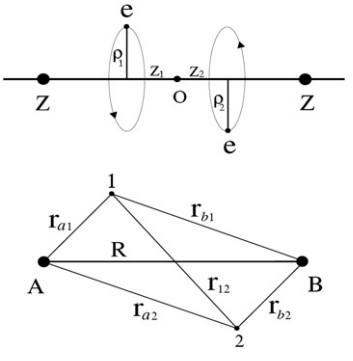

Figure 1. Cylindrical coordinates (top) and electronic distances (bottom) for H_2 molecule. The nuclei Z are fixed at a distance R apart. In the Bohr picture the two electrons rotate about the internuclear axis z with coordinates ρ_1, z_1 and ρ_2, z_2, respectively; the dihedral angle ϕ between the (ρ_1, z_1) and (ρ_2, z_2) planes remains constant at either $\phi = \pi$ or $\phi = 0$. The sketch corresponds to configuration 2 of Figure 8, with $\phi = \pi$.

in terms of distances defined in Figure 1. In cylindrical coordinates ($i=1,2$)

$$r_{ai}=\sqrt{\rho_i^2+\left(z_i-\frac{R}{2}\right)^2},\quad r_{bi}=\sqrt{\rho_i^2+\left(z_i+\frac{R}{2}\right)^2}, \tag{2.3}$$

$$r_{12}=\sqrt{(z_1-z_2)^2+\rho_1^2+\rho_2^2-2\rho_1\rho_2\cos\phi}, \tag{2.4}$$

where R is the internuclear spacing and ϕ the dihedral angle between the planes containing the electrons and the internuclear axis.

To generalize to D-dimensions, we endow each vector with D Cartesian coordinates. Thereby the potential energy V retains the same form as for $D=3$, but the Laplacian operators ∇^2 in the kinetic energy and the Jacobian volume element J are modified. We then transform the wavefunction by

$$\Psi=(\rho_1\rho_2)^{-(D-2)/2}\Phi, \tag{2.5}$$

and scale the coordinates by κ^2 and the energy by κ^{-2}, with $\kappa=(D-1)/2$. This recasts the Schrödinger equation, for Σ states, as

$$(T_1+T_2+U+V)\Phi=E\Phi, \tag{2.6}$$

where

$$T_1+T_2=\sum_{i=1,2}-\frac{2}{(D-1)^2}\left\{\frac{\partial^2}{\partial\rho_i^2}+\frac{\partial^2}{\partial z_i^2}+\frac{1}{\rho_i^2}\frac{\partial^2}{\partial\phi^2}\right\}, \tag{2.7}$$

and

$$U=\frac{(D-2)(D-4)}{2(D-1)^2}\left(\frac{1}{\rho_1^2}+\frac{1}{\rho_2^2}\right). \tag{2.8}$$

In the limit $D\to\infty$ the derivative terms T_i ($i=1,2$) in the kinetic energy are quenched, whereas the centrifugal portion U survives. The corresponding energy $E(D\to\infty)$ for any given internuclear distance R is then obtained simply as the extremum of the effective potential, $U+V$, given by

$$E=\frac{1}{2}\left(\frac{1}{\rho_1^2}+\frac{1}{\rho_2^2}\right)+V(\rho_1,\rho_2,z_1,z_2,\phi,R). \tag{2.9}$$

This is exactly the energy function for the Bohr model of H_2; in Section 3 we evaluate its extremum solutions and extensions to other molecules.

The D-scaling applied here differs from that used previously [14,35] only in how the dihedral angle ϕ is treated. The previous procedure employed the full Jacobian, $J=(\rho_1\rho_2)^{D-2}(\sin\phi)^{D-3}$, in transforming the wavefunction via $\Psi\to J^{-1/2}\Phi$, and likewise included corresponding ϕ-dependent factors in the Laplacian. In the large-D limit, the net result is that the energy function becomes

$$E=\frac{1}{2}\left(\frac{1}{\rho_1^2}+\frac{1}{\rho_2^2}\right)\frac{1}{\sin^2\phi}+V(\rho_1,\rho_2,z_1,z_2,\phi,R), \tag{2.10}$$

which differs from Equation (2.9) only by the factor $1/\sin^2\phi$ in the centrifugal term.

Our current procedure, designed to reduce to the Bohr model at the large-D limit, retains the $D=3$ form for the ϕ-part of both the Jacobian and Laplacian. This has important consequences. Figure 2 displays the ground state $E(R)$ functions for the large-D limit obtained from Equations (2.9) and (2.10). Whereas the Bohr model version (solid curve) gives a good zero-order approximation, the 'full-J' version (dashed curve) fails to exhibit binding. Also shown is the substantial improvement to the Bohr result obtained from a simple interpolation correction (described in Section 3; see Figure 9).

In essence, D-scaling procedures resemble gauge transformations. Many varieties of scaling are feasible, subject only to the constraint that as $D \to 3$ the scaled Schrödinger equation reduces to the correct form. The basic aim is to devise a scaling that removes the major, generic D-dependence, enabling the easily evaluated $D \to \infty$ limit to approximate the $D=3$ energy. With the 'full-J' scaling previously used [35], when D is increased the $(\sin\phi)^{D-3}$ factor in the Jacobian forces ϕ towards 90°, while minimization of electron–electron repulsion requires $\phi \to 180°$. The effect is to overweight electron repulsion; this is a chief source of the failure to obtain chemical bonding from Equation (2.10). In Section 5 we discuss further aspects of variant scalings. In our 'Bohr-scaling' variant ϕ remains a fully quantum variable as $D \to \infty$ rather than being converted to a semiclassical parameter along with the ρ and z coordinates. This avoids overweighting electron repulsion and hence favours chemical bonding.

The scaling procedure enables, in the large-D limit, calculations to be carried out in the scaled space that are entirely classical. The extremum equations, $\partial E/\partial z = 0$ and $\partial E/\partial \rho = 0$, are identical to classical equilibrium configurations under Newton's second law. Although the electrons are thereby confined to specific orbits in the scaled space, the uncertainty principle is nonetheless satisfied. This is so because the conjugate momenta are scaled inversely to the coordinates, leaving the position-momentum commutator invariant.

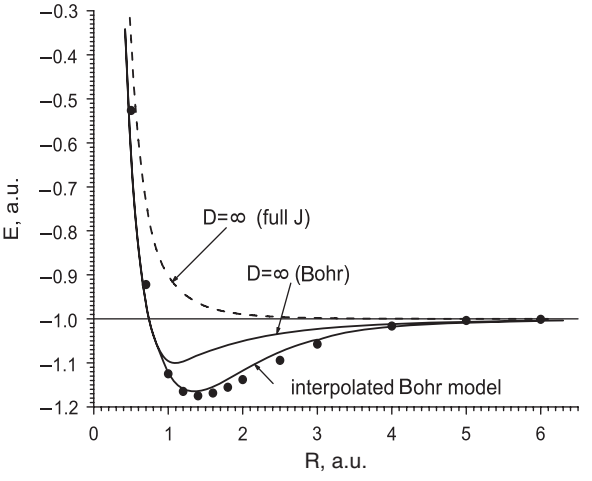

Figure 2. Intermolecular potential energy curves $E(R)$ for electronic ground state of H_2 in the $D \to \infty$ limit, obtained from Equation (2.9) for Bohr model (solid curve) and from Equation (2.10) for 'full-J' scaling (dashed curve). Also shown (lower solid curve) is an improvement obtained by an interpolation method described in Section 3 (see Figure 9). Dots show accurate $D=3$ results obtained from high-quality wavefunctions [36,37].

The continuous transition between the scaled space and the unscaled space in effect relates classical trajectories at large-D to corresponding quantum distributions at $D=3$. This aspect becomes particularly evident when treating electronic tunnelling [14].

Figure 3 displays the electron charge density along the molecular axis in the ground state of H_2 for internuclear spacing $R=0.8$ and 1.4 a.u., as obtained from $D=3$ Hund–Mulliken wavefunction [38]. Circles show electron orbits in Bohr's model. As shown in Figure 4, the orbit locations for any R are actually very close to the maxima in the charge density. This provides a satisfying link between the wave mechanical and large-D limit Bohr model treatments of the H_2 bond.

The ground state $E(R)$ can be substantially improved by use of a simple interpolation procedure (see Figure 9). We discuss this in Section 3. The present $D\to\infty$ limit (Bohr model) gives good results for other molecules; examples we include in this review are HeH, He_2, LiH, BeH, Li_2, and the triatomic H_3.

2.2. *Bohr model picture of multielectron atoms*

While Bohr's model gives exact energies of one-electron atoms, when extended to the helium atom it gave disappointing results (ionization energy 15% too high). There were several further attempts to obtain better classical mechanical many-electron models, relying on physical intuition. Parson [39] suggested that in many atoms the electrons are arranged with cubic symmetry. Lewis [40] emphasized the importance of pairs and octets of electrons. Kossel [41] found certain unusually stable groupings of electrons in atoms, corresponding to the inert gases. Born [42] and Landé [43–47] demonstrated stable octets of electrons and analysed the motion of the octets about certain points.

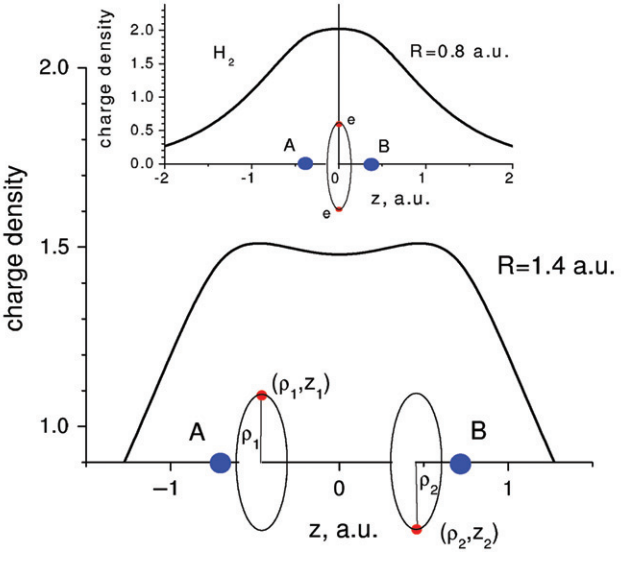

Figure 3. Distribution of the electron charge density in the ground state of H_2 along the molecular axis z, obtained from a Hund–Mulliken wavefunction [38]. The nuclei are fixed a distance R apart. Circles are electron orbits in Bohr's model.

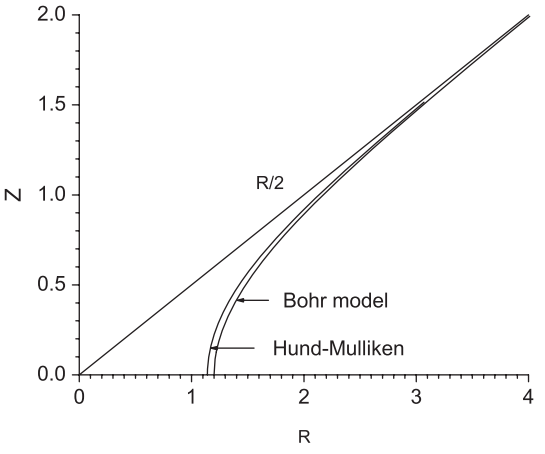

Figure 4. Location of the peak (relative to the centre) in the ground state charge density of H_2 molecule as a function of R. Curves were calculated from the Bohr model of Equation (2.9) and from the Hund–Mulliken variational wavefunction with effective charge [38].

Langmuir postulated a set of rules for coupling of electrons in atoms [48]. Since in the ground state the total angular momentum is zero, the momenta of an electron pair must be equal and opposite. Subject to this requirement, Langmuir considered oscillatory motions of electrons along semicircular orbits in the equatorial plane [48]. For helium, he obtained an ionization energy (0.945 hartrees) close to the experimental value. Harcourt [49] modified Bohr's model for He so that the electrons could deviate from being 180° apart in their orbits and obtained an accurate ground-state energy. Contemporary semiclassical theory of electronic orbits in atoms has a sound mathematical foundation [50]. It has given good results both for doubly excited Rydberg atoms and for frozen planetary states [51]. West, *et al.* [52] have also studied classical orbits for helium using the techniques of Rydberg electronic wave packets.

Our new perspective on the Bohr model encourages looking into how it might work for many-electron atoms. We consider here a simplistic approach, akin to Equation (2.9), for the lowest S state configurations of atoms. In his 1913 model for a one-electron atom, Bohr postulated circular electron orbits with radii determined by $r = n/p$ (in atomic units), with n the principal quantum number, p the momentum [29–31]. Then minimizing the energy,

$$E = \frac{1}{2}p^2 + V = \frac{1}{2}\frac{n^2}{r^2} - \frac{Z}{r}, \tag{2.11}$$

with Z the nuclear charge, gives $E = -\frac{1}{2}Z^2/n^2$. By analogy, we might expect that for the ground S states of an N-electron atom, the Bohr model energy function should be

$$E = \frac{1}{2}\sum_{i=1}^{N}\frac{n_i^2}{r_i^2} + V(\mathbf{r}_1, \mathbf{r}_2, \ldots, \mathbf{r}_N), \tag{2.12}$$

where $r_i (i = 1, \ldots, N)$ is the distance from the electron i to the nucleus, n_i is the principal quantum number of electron i and V is the Coulombic potential energy. For $N = 2$,

this function indeed agrees with the united atom limit ($R=0$) of Equation (2.9). In Section 6, we show that Equation (2.12) can be obtained from an extended D-scaling procedure. For now, just proceeding blithely, we assign the quantum numbers for each electron using the familiar prescription for sequential filling of the K, L, M... ($n=1,2,3,\ldots$) energy shells, with $2n^2$ the maximum occupation number of each shell.

Figure 5 shows the electron configurations obtained by minimizing Equation (2.12) for neutral atoms with $N=2$ to 6. These represent, at a modest level of approximation, the fixed geometry that the electrons attain at the large-D limit. The electron locations agree remarkably well with the radius of maximum radial charge density in atomic shells and subshells, determined from $D=3$ self-consistent-field calculations using the Roothaan–Hartree–Fock (RHF) wavefunction taken from [53]. For the $n=1$ shell, the radii shown in Figure 5 are actually identical to the RHF most probable radii (0.569, 0.36, 0.26, 0, 21, 0.17, respectively). For the $n=2$ shell, the Bohr result for Li (3.85) is much larger than the RHF value (3.09), but for Be, B, and C the agreement with RHF data (2.04, 1.53, 1.21, respectively) is good.

Another striking aspect of Figure 5 is that simply minimizing Equation (2.12) predicts that in the $n=2$ shell the valence electrons for Be, B, and C will be disposed in linear, trigonal, or tetrahedral geometry, respectively. These configurations correspond to the sp, sp^2, and sp^3 modes of hybridization of the s and p subshells. Championed by Pauling and Slater, orbital hybridization is invoked in myriad discussions of chemical bonding [54–57]. Conventional treatments of hybridization, using $D=3$ wave mechanics, need to call on special approximations to obtain these canonical modes, so it is interesting that in the Bohr model they appear without ado.

Figure 6 shows, for neutral atoms with $N=Z=2$ to 30, how much the ground state energies found by minimizing Equation (2.12) deviate from accurate results of high-level calculations (accurate atomic energies were obtained from Hartree–Fock energies of [58–61] and correlation energies [62,63]). The accuracy of E_{Bohr} is much less good than obtained from Hartree–Fock calculations [60–63]. That is to be expected for such a simplistic model, but contrasts with the results of Figure 5. For $N=2$, our procedure is equivalent to Bohr's model of He, in which the electrons revolve about the nucleus in a common circular orbit. That model overestimates the He energy by nearly 6%. For $N>2$, as evident in Figure 5, our version defined by Equation (2.12) differs from Bohr's original model [64]; his continued to employ coplanar, concentric circular orbitals and for Li and Be gave even poorer energy results [65]. Recently, Sergeev has examined the behaviour of our version of $E_{\mathrm{Bohr}}(N,Z)$ as $N=Z$ becomes very large [66]. He found the functional form of the Z-dependence became similar to the Thomas–Fermi statistical model [67]. He also demonstrated an enhanced minimization procedure. He noted that the procedure usually used actually treats Equation (2.12) as if the electron vectors are in 3D space. When instead he did the minimization in successively larger-D spaces, he found the electronic shells became increasingly symmetric, until at sufficiently large D each shell forms a simplex, with all electrons in the same shell at the same distance from the nucleus. That simplified the calculations and also, as seen in Figure 6, at large-N increased the accuracy of E_{Bohr} by roughly twofold. For comparison, Figure 6 includes results obtained from the Thomas–Fermi model and from Loeser's approximate large-D limit [68].

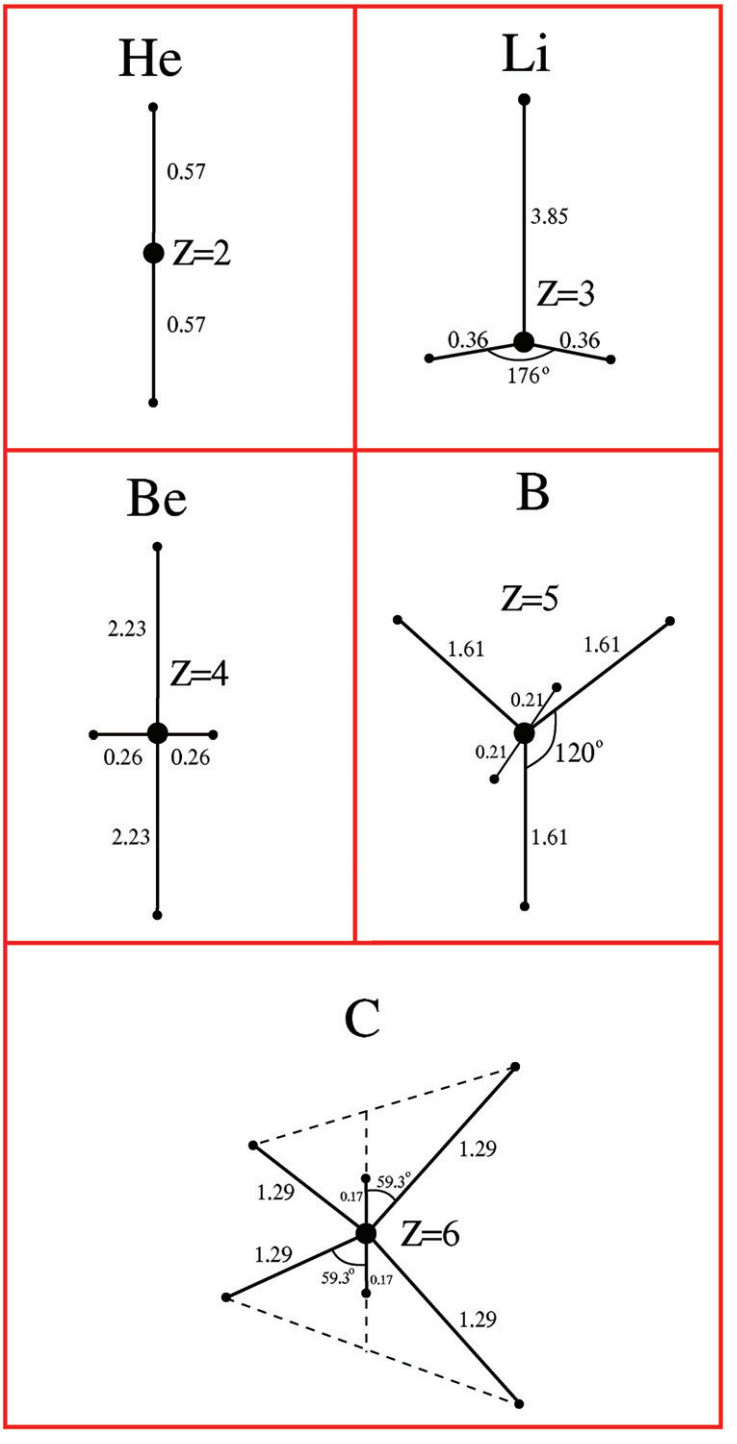

Figure 5. Electron configurations obtained from Bohr model by minimizing Equation (2.12). Distances in atomic units (1 a.u. = 0.529 Å).

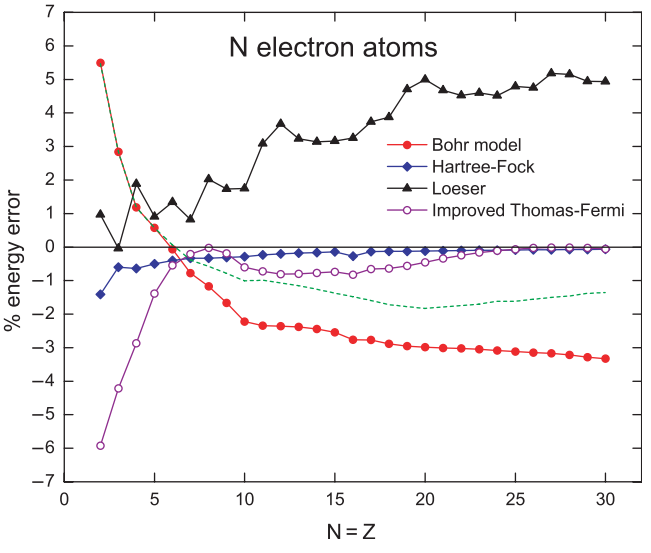

Figure 6. Deviation of ground state energy of multielectron atoms obtained from the Bohr model of Equation (2.12) from the accurate high-level quantum mechanical result (accurate atomic energies were obtained from Hartree–Fock energies of [58–61] and correlation energies [62,63]). For comparison, data are shown also for the Hartree–Fock approximation [58–61], the Thomas–Fermi statistical model [67], and Loeser's approximate large-D limit [68]. Dashed curve shows improved results for the Bohr model obtained by Sergeev [66].

3. Chemical bond in Bohr model picture

From 1913 on, Bohr hoped to elucidate molecular as well as atomic electronic structures. Figure 7, from an unpublished manuscript [69], displays the 'figurations' he considered for H_2 and other simple molecules. Even for H_2, none of the various planetary-orbit models examined during the 'old quantum theory' appeared able to account for chemical bonding. Textbooks thus have long credited the first theoretical explanation of a covalent bond to the approximate wave mechanical treatment of H_2 in 1927 by Heitler and London [70]. We now find, however, that a simple extension of the original Bohr model actually describes the potential energy curves for the lowest singlet and triplet states of H_2 about as well as the results of Heitler and London. The Bohr model also proves to work well for other small diatomic molecules.

3.1. *The hydrogen molecule*

In his unpublished notes, referring to Figure 7, Bohr says 'The model proposed for H_2 seems to be the only possible equilibrium configuration of 2 kerns and 2 electrons (looking apart from two atoms), in which the kerns are at rest'. However, the symmetric configuration he considered is the minimum energy solution of Equation (2.9) only at small internuclear distances. Figure 8 shows all possible stationary configurations. Apparently, Bohr was unaware of the asymmetric configurations, displayed in our Figure 8. Combining his solution (curve 1) at small R with an asymmetric one (curve 2) that gives the minimum energy at larger R provides a fair first approximation to the

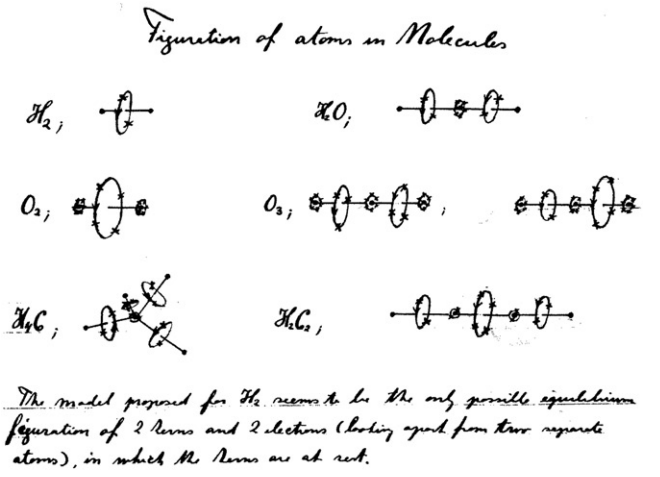

Figure 7. Molecular configurations as sketched by Niels Bohr; from an unpublished manuscript [69], intended as an appendix to his 1913 papers.

ground state potential energy over the full range of R. Arnold Sommerfeld, who in 1916 enhanced Bohr's H atom model by treating elliptical orbits, space quantization, and relativistic fine structure, had an apt premonition about the symmetric H_2 model. In the 1923 edition of Sommerfeld's 'quantum theory almanac', he comments that 'Only a short while ago... we were inclined to accept it... [but] nowadays we can take only a historical interest in it... Thus the true model of the H_2 molecule is still unknown. It will hardly be as symmetrically built as the model exhibited [by Bohr in Figure 7].'

As depicted in Figure 1, the Bohr model for H_2 assumes that the electrons move with constant speed on circular orbits of radii $\rho_1 = \rho_2$. The centres of each orbit lie on the molecular axis z at positions $z_1 = \pm z_2$. The dihedral angle ϕ between the planes containing the molecular axis and the electrons is either 180° or zero, $\phi = \pi$ or $\phi = 0$. Thus, the pair of electrons rotate synchronously, and the separation between them remains constant. In Figure 8, the upper panel shows the four electron configurations that correspond to extrema of the Bohr energy function of Equation (2.9). The lower panel plots the four corresponding potential energy curves, $E(R)$. Also shown (dots) are accurate results obtained from high quality wave mechanical calculations for the singlet ground state, $^1\Sigma_g^+$ and the lowest triplet state, $^3\Sigma_u^+$ [36,37]. In the model, the three configurations 1, 2, 3 with the electrons on opposite sides of the internuclear axis ($\phi = \pi$) are seen to correspond to singlet states, whereas the other solution 4 with the electrons on the same side ($\phi = 0$) corresponds to the triplet state. (The latter is a saddle point of Equation 2.9, the others are minima.) At small internuclear distances, the symmetric configuration 1 originally considered by Bohr agrees well with the accurate ground state quantum energy; at larger R, however, this configuration climbs far above the ground state and ultimately dissociates to the doubly ionized limit, $2H^+ + 2e$. In contrast, the solution for the asymmetric configuration 2 appears only for $R > 1.20$ and in the large R limit dissociates to two H atoms. The solution for asymmetric configuration 3 exists only for $R > 1.68$ and climbs steeply to dissociate to an ion pair, $H^+ + H^-$. The asymmetric solution 4 exists for all R and corresponds throughout to repulsive interaction of two H atoms.

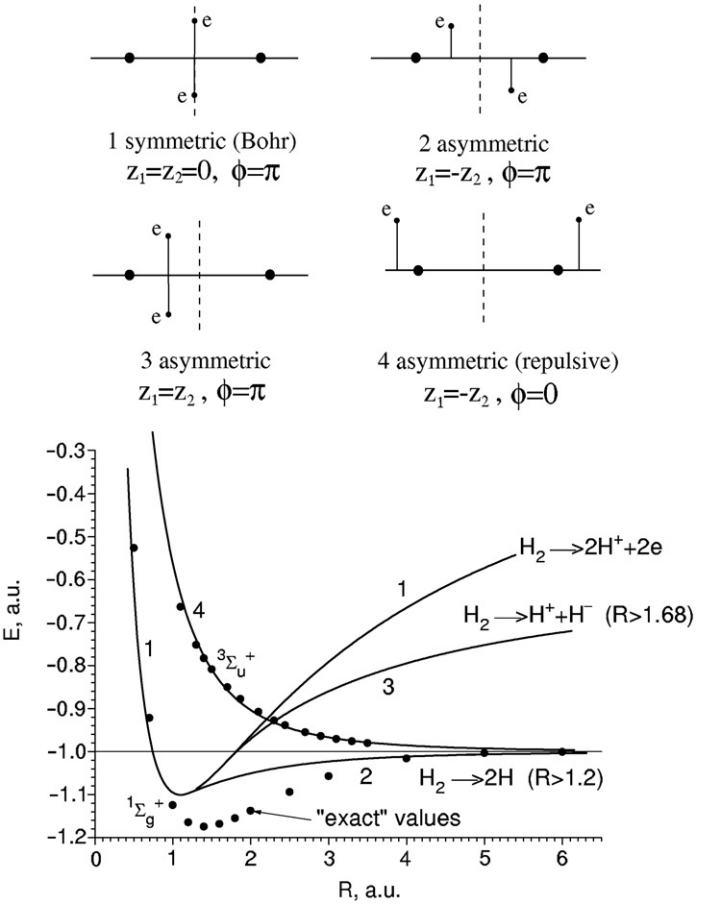

Figure 8. Energy $E(R)$ of H_2 molecule for four electron configurations (top) as a function of internuclear distance R calculated within the Bohr model (solid curves) and the accurate ground $^1\Sigma_g^+$ and first excited $^3\Sigma_u^+$ state energy (dots) [36,37]. Unit of energy is 1 a.u. = 27.21 eV, and unit of distance is the Bohr radius. Note the symmetric configuration 1 corresponds to Bohr's sketch of H_2 molecule in Figure 7.

In the united atom limit $R=0$, the configuration 1 turns into the $\theta=180^\circ$ configuration for the Bohr model of helium. The configuration 4 in this limit turns into the rigid triangle configuration for the Langmuir model of helium, in which two electrons rotate in the same direction in circular orbits in two parallel planes equidistant from the equatorial plane [34]. Both orbits in helium are classically unstable [52]. More various types of orbits like Bohr's and Langmuir's orbits for the helium atom were found for the hydrogen molecule by Lopez-Castillo [71].

The simplistic Bohr model provides surprisingly accurate energies for the ground singlet state at large and small internuclear distances and for the triplet state over the full range of R. Also, the model predicts the ground state is bound with an equilibrium separation $R_e \approx 1.10$ and gives the binding energy as $E_B \approx 0.100$ a.u. = 2.73 eV. The Heitler–London calculation, obtained from a two-term variational function, gives

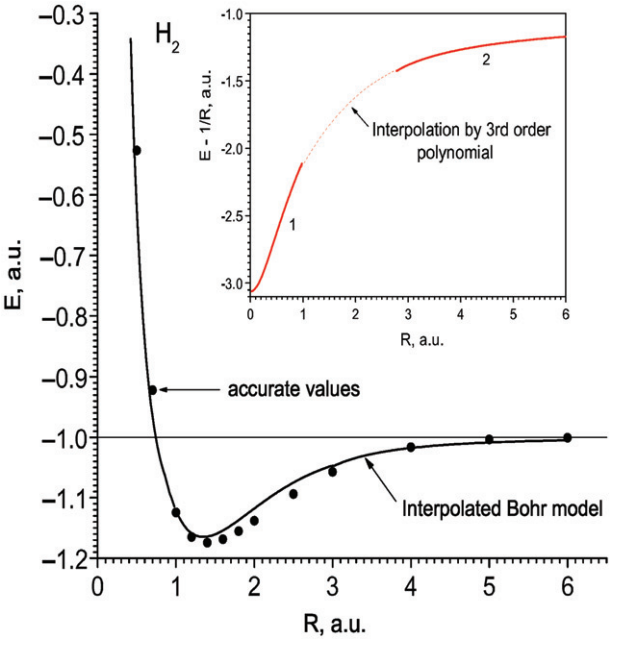

Figure 9. Ground state potential energy $E(R)$ of H_2 molecule calculated from the interpolated Bohr model (solid curve) and the accurate energy (dots) [36,37]. Insert shows $E(R)$ with no $1/R$ term. Curves 1 and 2 are obtained based on the quantization relative to the molecular axis (small R) and the nearest nuclei (large R) respectively. Dashed line is the interpolation between two regions.

$R_e = 1.51$ and $E_B = 3.14\,\text{eV}$ [70], whereas the accurate results are $R_e = 1.401$ and $E_B = 4.745\,\text{eV}$ [1,2]. For the triplet state, as seen in Figure 8, the Bohr model gives remarkably close agreement with the accurate potential curve and is in fact much better than the Heitler–London result, which, e.g., is 30% high at $R = 2$.

In order to emphasize how simple the Bohr model calculations are, in contrast to solving the Schrödinger equation, we consider configuration 2 as an example. There $z_1 = -z_2 = z$, $\phi = \pi$, and the extremum conditions $\partial E/\partial z = 0$ and $\partial E/\partial \rho = 0$ read

$$\frac{Z(R/2-z)}{\left[\rho^2+(R/2-z)^2\right]^{3/2}} + \frac{z}{4[\rho^2+z^2]^{3/2}} - \frac{Z(R/2+z)}{\left[\rho^2+(R/2+z)^2\right]^{3/2}} = 0, \tag{3.1}$$

$$\frac{Z\rho}{\left[\rho^2+(R/2-z)^2\right]^{3/2}} + \frac{Z\rho}{\left[\rho^2+(R/2+z)^2\right]^{3/2}} - \frac{\rho}{4[\rho^2+z^2]^{3/2}} = \frac{1}{\rho^3}. \tag{3.2}$$

These are seen to be identical to classical equilibrium configurations under Newton's second law. Equation (3.1) specifies that the total Coulomb force on the electron along the z-axis is equal to zero; Equation (3.2) specifies that the projection of the Coulomb force toward the molecular axis equals the centrifugal force. At any fixed internuclear distance R, these algebraic equations determine the constant values of ρ and z that describe the electron trajectories. Substituting these values back into Equation (2.9) yields $E(R)$. Similar force equations pertain for the other extremum configurations.

We have found an easy way to improve significantly the Bohr model result for the ground state $E(R)$ of H_2. His model, leading to Equation (2.9), assumes quantization of the electron angular momentum relative to the molecular axis. As seen in Figure 8, this yields quite accurate results for R up to nearly 1 a.u. but becomes much less good at larger internuclear separation. At large R, however, each electron feels almost only the nearest nuclear charge. Thus, at large R, we should find that quantization of the momentum relative to the nearest nucleus, rather than to the molecular axis, should provide a better description of the physics. This leads to replacing Equation (2.9) at large R by the following expression,

$$E = \frac{1}{2}\left(\frac{1}{r_{a1}^2} + \frac{1}{r_{b2}^2}\right) + V(r_{a1}, r_{b1}, r_{a2}, r_{b2}, r_{12}, R). \tag{3.3}$$

For $R > 2.77$ a.u. this expression has a local minimum for the asymmetric configuration 2 of Figure 8. We plot in Figure 9 (insert, curve 2) the corresponding $E(R)$, without the $1/R$ term. The local minimum of Equation (3.3) disappears at $R < 2.77$ and the electrons collapse into the opposite nuclei. Therefore, at $R < 1$ we apply Equation (2.9), with its quantization relative to the molecular axis (insert, curve 1). At intermediate R, we smoothly connect the $R < 1$ and $R > 2.77$ regions by a third-order interpolating polynomial (dashed curve). Addition of the $1/R$ term then gives the final potential curve, plotted in Figure 9. This interpolated version of the Bohr model indeed provides good agreement with the accurate $E(R)$ curve over the full range of R. In Section 4 we present a strategy that avoids interpolation but likewise enhances accuracy by switching quantization from molecular to atomic as R increases.

Another simple strategy, combining the large-R result for H_2 with the exact $E(R)$ for the ground state H_2^+ molecule-ion, enables estimating potential energy curves for some H_2 excited states. For small R, an excited electron (denoted 2) with principal quantum number $n_2 \geq 2$ will mostly be far from its companion (with $n_1 = 1$) and both protons. Therefore, the itinerant electron 2 feels an effective charge nearly equal to +1, so its energy is well approximated as hydrogenic, with $E(H, n_2) = -1/2n_2^2$. The inner electron 1 will feel almost as if it is in a H_2^+ ion. Hence potential energy curves of such excited H_2 states can be approximated as

$$E(R; H_2) = E\big(R; H_2^+, n_1 = 1\big) + E(H, n_2) \tag{3.4}$$

As shown in Figure 10, this yields a fairly accurate result for the $2s\sigma$ state in the vicinity of its first minimum and even a rough indication of the unusual double-well character. For the $3s\sigma$ and $4s\sigma$ states the results are better and remain accurate over a wide range of R.

3.2. *Other simple diatomic molecules*

By means of the same procedure leading to Equation (2.12), the rudimentary Bohr model for H_2 can be generalized to apply to Σ states of an N-electron diatomic molecule. This gives

$$E = \frac{1}{2}\sum_{i=1}^{N} \frac{n_i^2}{\rho_i^2} + V(\mathbf{r}_1, \mathbf{r}_2, \ldots, \mathbf{r}_N, R), \tag{3.5}$$

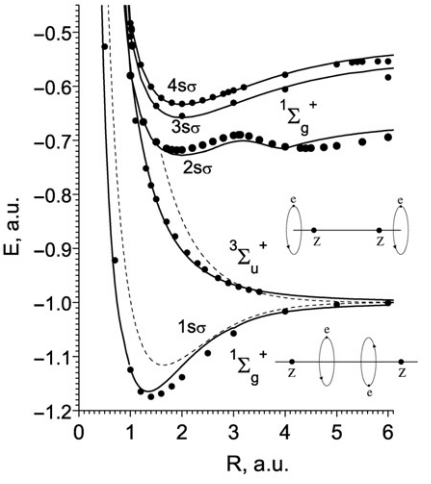

Figure 10. Potential energy (solid curves) of the ground and a few excited states of H_2 obtained from the Bohr model with D-scaling analysis. Dots are the accurate energies [72]. The inserted figures on the right hand side depict the two nuclei of charge Z and Bohr's 'planetary' orbits for the electrons in the $^1\Sigma_g^+$ and $^3\Sigma_u^+$ states (see also Figure 3). Dashed curves are from Heitler–London treatment [70]. Taken from [34].

where the ρ_i coordinates are replaced by r_i when we desire to switch from molecular to atomic quantization. As before, we seek configurations that deliver extrema of this energy function, and incorporate Pauli exclusion by assigning the principal shell quantum numbers n_i in the usual way.

Figure 11 shows for HeH the ground state electron configuration and repulsive $E(R)$ curve obtained from Equation (3.5) with $n_1 = n_2 = n_3 = 1$. Here we find molecular quantization remains appropriate even at large R, as the model dissociates properly to He + H. In order to correct for the error in the Bohr result for He, we reduce the effective nuclear charge to $Z_{\mathrm{He}}^{\mathrm{eff}} = 1.954$ and thereby fit the correct dissociation limit. With this adjustment, the Bohr model gives remarkably close agreement with the accurate potential curve for HeH.

Figure 12 pertains to He_2, another case for which the ground state potential curve is repulsive. For simplicity, here we assumed a symmetrical collinear electron configuration (depicted in the insert) and used momentum quantization relative to the nearest nucleus. Then the Bohr energy function to be minimized becomes

$$E(r_1, r_2, R) = \frac{1}{r_1^2} + \frac{1}{r_2^2} - \frac{2Z}{r_1} - \frac{2Z}{r_2} - \frac{2Z}{R + r_1} - \frac{2Z}{R - r_2} + V_{ee} + \frac{Z^2}{R}, \tag{3.6}$$

where the electron–electron interactions are

$$V_{ee} = \frac{2}{r_1 + r_2} + \frac{2}{R + r_1 - r_2} + \frac{1}{R + 2r_1} + \frac{1}{R - 2r_2}. \tag{3.7}$$

The $E(R)$ curve thereby obtained, again with adjustment of the large-R asymptote to the correct dissociation limit, agrees very closely with the accurate curve found from extensive wave mechanical calculations.

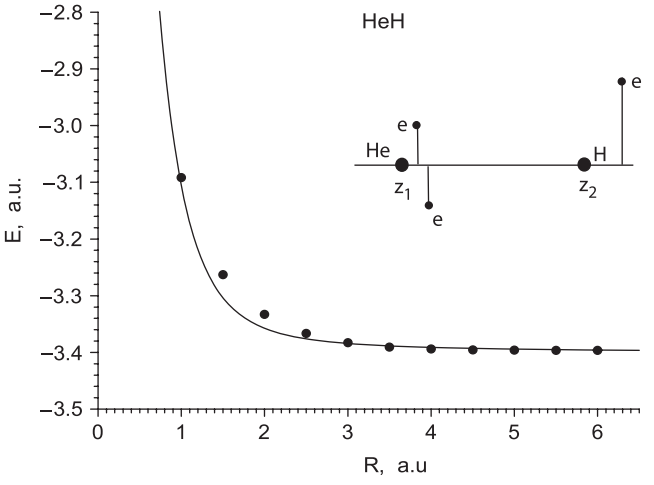

Figure 11. Ground state potential energy $E(R)$ of HeH molecule for the shown electron configuration, calculated from the Bohr model with $n_1 = n_2 = n_3 = 1$, $Z_{He}^{eff} = 1.954$ (solid curve) and compared with the accurate ground state energy (dots) [73].

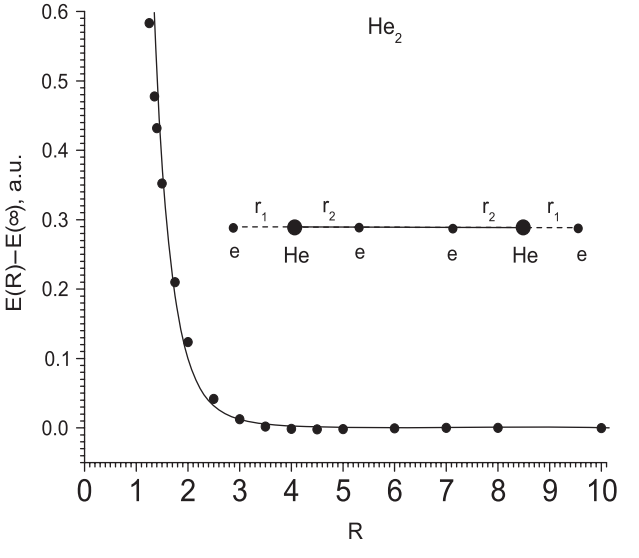

Figure 12. Ground state potential energy $E(R)$ of He_2 molecule calculated from the Bohr model (solid curve) and compared with the accurate energy (dots) [74–76]. Insert shows the electron configuration.

Figure 13 for LiH returns to treating a ground state that has chemical bonding. Here we simplified by relegating the two inner shell electrons of Li to the configuration found in Figure 5, so considered just the $n = 2$ outer electron of Li as involved in the bond with the electron from H. Then we evaluated $E(R)$ using interpolation (as for H_2 in Figure 9) between results obtained with quantization with respect to the molecular axis at small R

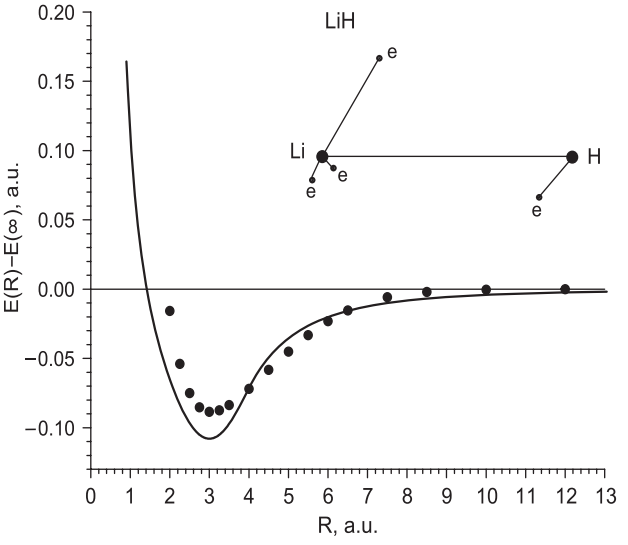

Figure 13. Electron configuration and the ground state energy $E(R)$ of LiH molecule as a function of internuclear distance R calculated from the interpolated Bohr model (solid curve) and compared with the accurate energy (dots) [77].

and with respect to the nearest nucleus at large R. This 'minimalist' treatment again gives fairly good agreement with the accurate potential curve. From the Bohr model perspective, the essential difference from H_2 arises just because in LiH the $n=2$ electron contributed by Li is much less strongly bound than the $n=1$ electron from H. Consequently, for LiH the bond energy is about twofold smaller than of H_2 and the equilibrium bond length roughly twice as large. As seen in Figure 14, we find that the same procedure applied to BeH also gives good results.

Figure 15 displays a potential curve for Li_2 obtained by another 'minimalist' stratagem. If we freeze or neglect the inner-shell electrons, the Bohr model Li_2 becomes equivalent to a pseudo-H_2 state with $n_1=n_2=n=2$. Rescaling coordinates in Equation (3.3) via $r\to n^2 r$ and $R\to n^2 R$ then rescales the energy function by n^{-2}. Hence, the ground state potential curve of Li_2 can be estimated from that for H_2 using a simple relation,

$$E_{Li_2}(R)-E_{Li_2}(\infty)=\frac{1}{n^2}\left[E_{H_2}(n^2R)-E_{H_2}(\infty)\right]. \tag{3.8}$$

As seen in Figure 15, the result agrees fairly well with the accurate potential curve. Although the Bohr potential well is wider, its depth (1.10 eV) is quite close to the accurate bond strength (1.05 eV).

As indicated by these examples, when applied with suitably judicious approximations, the Bohr model can readily provide surprisingly accurate potential energy curves. More important, it offers a clear physical picture for prototypical chemical bonding, a picture consistent with but much more elementary than that provided by wave mechanics.

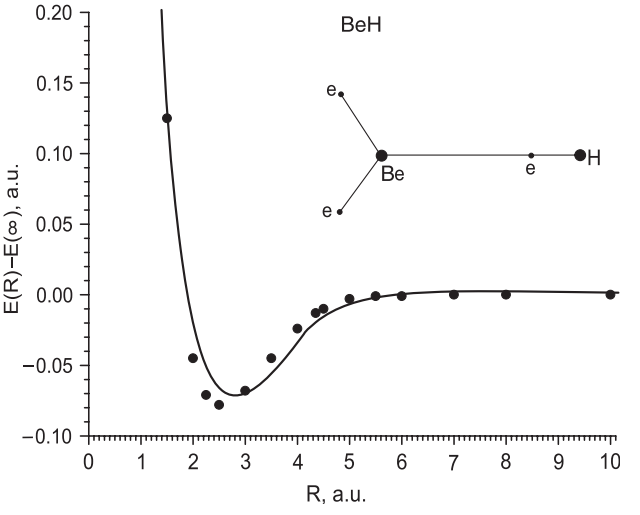

Figure 14. Ground state potential energy $E(R)$ of BeH molecule calculated from the interpolated Bohr model (solid curve) and compared with the accurate energy (dots) [78]. Insert shows the electron configuration at large R; only outer-shell Be electrons are displayed.

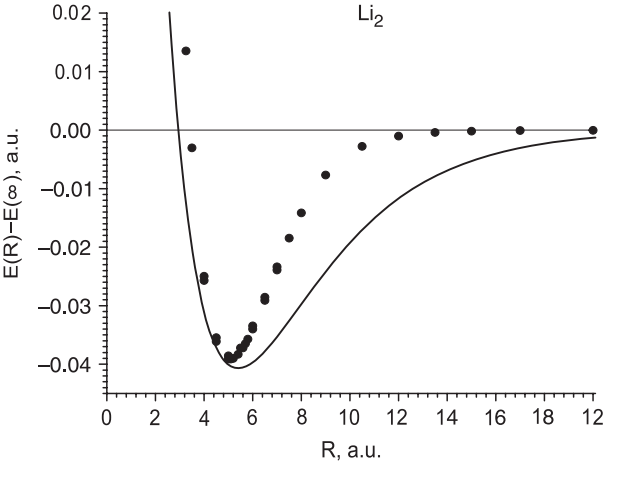

Figure 15. Ground state potential energy $E(R)$ of Li_2 molecule calculated from the interpolated Bohr model (solid curve) and compared with the accurate energy (dots) [79,80].

4. Constrained Bohr model approach

Here we introduce a method which augments the Bohr model with a constraint imposed by quantum mechanics [81]. Thereby it avoids the arbitrariness of interpolation. The constraint is as simple and intuitively appealing as the original Bohr model, yet proves capable of giving quite accurate potential energy curves.

We first discuss the method as applied to H_2, and then extend it to other molecules. In Section 3.1, in presenting the interpolation expedient of Figure 9, we described why it is

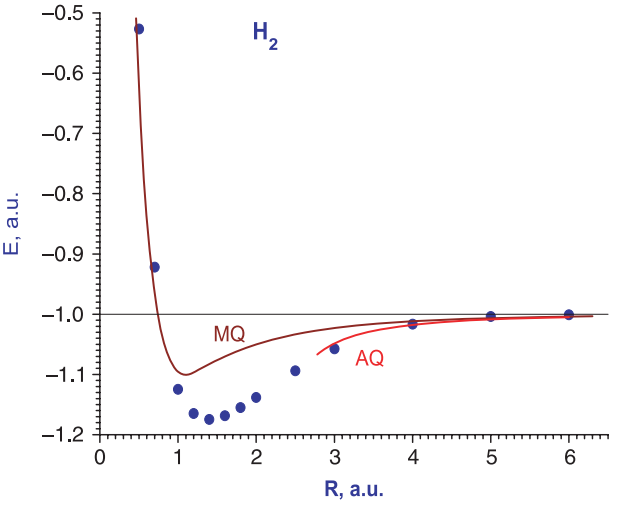

Figure 16. Potential energy curve for the ground state of the H_2 obtained from the Bohr model using molecular axis quantization (curve labelled MQ) or using quantization relative to the nearest nucleus (curve AQ). Dots show results from accurate calculations [36,37].

appropriate at small R to use momentum quantization with respect to the molecular axis (MQ), but at large R to use quantization with respect to the nearest atomic nucleus (AQ). The switch involves changing the centrifugal portion of the Bohr energy function from

$$\text{MQ: } \frac{1}{2}\left(\frac{1}{\rho_1^2}+\frac{1}{\rho_2^2}\right) \quad \text{to} \quad \text{AQ: } \frac{1}{2}\left(\frac{1}{r_1^2}+\frac{1}{r_2^2}\right), \tag{4.1}$$

which converts Equation (2.9) to Equation (3.3); again, we use the notation of Figure 1. The $E(R)$ curves given by the MQ and AQ versions are compared in Figure 16. Whereas the Bohr AQ version is accurate when the atoms are far apart, it fails as R decreases because both electrons collapse onto the neighbouring nuclei. This occurs because the neighbours exert increasing Coulombic attractions ($-1/r_{b1}$ and $-1/r_{a2}$ terms) but there are no corresponding Bohr kinetic energy terms to prevent the collapse. We derive now, in a simple algebraic form, the quantum constraint on electron locations that removes this instability and enables the Bohr AQ version to be used over the full range of R.

4.1. *Effective constraint potential for H_2*

Quantum mechanics describes the two electrons in H_2 by a wavefunction, $\Psi(\mathbf{r}_1, \mathbf{r}_2)$. Electron 1 is a charge cloud with a most probable radius r. Let $\Phi(r, R)$ be the quantum potential between the electron 1 cloud centred at nucleus A and the neighbouring nucleus B (or vice versa for electron 2). In the Bohr picture we treat the electron as a point particle on a sphere of radius r centred about nucleus A. On the sphere surface, a subset 'circle' of positions r satisfying $-1/r_{b1} = \Phi(r, R)$ will give the correct quantum interaction energy with nucleus B. If we impose this as a constraint, and choose the electron location only from this subset, then r_{b1} can never collapse to zero because $\Phi(r, R)$ is finite.

The effective potential $\Phi(r, R)$ can be derived from any two-electron wavefunction. Here we consider just the prototype valence-bond and molecular orbital functions: Heitler–London (HL) and Hund–Mulliken (HM), respectively [38,70]. The HL wavefunction is defined by

$$\Psi_{\mathrm{HL}} = a(1)b(2) \pm b(1)a(2), \tag{4.2}$$

where '+' pertains to the singlet state, '−' to the triplet state, and

$$a(i) = \sqrt{\frac{\alpha^3}{\pi}}\exp(-\alpha r_{ai}), \quad b(i) = \sqrt{\frac{\alpha^3}{\pi}}\exp(-\alpha r_{bi}), \tag{4.3}$$

for $i = 1, 2$ are variational wavefunctions with parameter α. If we take $a(1)$ for an isolated hydrogen atom, then the variational energy is $E = \alpha^2/2 - \alpha$. This expression reduces to the Bohr model energy function of the hydrogen atom if we identify $\alpha = 1/r$, where r is the radial distance from the nucleus. For molecules we will also use this assignment of α with r the radial distance of an electron from its nearest nucleus.

The singlet state HM wavefunction is

$$\Psi^s_{\mathrm{HM}} = [a(1) + b(1)][a(2) + b(2)], \tag{4.4}$$

For the triplet state, the HM and HL wavefunctions are the same, because the spatial wavefunction must be antisymmetric to exchange of either the electrons or the protons,

$$\Psi^t_{\mathrm{HM}} = \Psi^t_{\mathrm{HL}} = a(1)b(2) - b(1)a(2). \tag{4.5}$$

Let us consider the interaction potential of electron 1 with nuclei A and B. Using the HL wavefunction we find after simple transformations

$$\left\langle \Psi \middle| -\frac{1}{r_{b1}} - \frac{1}{r_{a1}} \middle| \Psi \right\rangle = -\frac{1}{1 \pm \left[\int a(1)b(1)\mathrm{d}\mathbf{r}_1\right]^2}\left[\int a^2(1)\frac{1}{r_{b1}}\mathrm{d}\mathbf{r}_1 \pm \int a(1)b(1)\frac{1}{r_{b1}}\mathrm{d}\mathbf{r}_1 \int a(2)b(2)\mathrm{d}\mathbf{r}_2 \right.$$
$$\left. \pm \int a(1)b(1)\frac{1}{r_{a1}}\mathrm{d}\mathbf{r}_1 \int a(2)b(2)\mathrm{d}\mathbf{r}_2 + \int a^2(1)\frac{1}{r_{a1}}\mathrm{d}\mathbf{r}_1\right]. \tag{4.6}$$

One can interpret the first two terms in Equation (4.6) as the interaction potential between nucleus B and the electron cloud localized at nucleus A. The last two terms describe the interaction potential between the electron cloud and nucleus A. Hence, $\Phi(r, R)$ is given by the first two terms in Equation (4.6). Similar analysis applies to the HM wavefunction. As a result, the HL and HM versions of the constraint function $\Phi(r, R)$ are given by

$$\Phi_{\mathrm{HL}} = -\frac{f(r, R) \pm S(r, R)g(r, R)}{1 \pm S^2}, \tag{4.7}$$

$$\Phi^s_{\mathrm{HM}} = -\frac{f(r, R) + g(r, R)}{1 + S}, \tag{4.8}$$

with

$$f(r, R) = \int a^2(1)\frac{1}{r_{\mathrm{b1}}}\mathrm{d}\mathbf{r}_1 = \frac{1}{R} - \exp\left(-\frac{2R}{r}\right)\left(\frac{1}{r} + \frac{1}{R}\right),$$

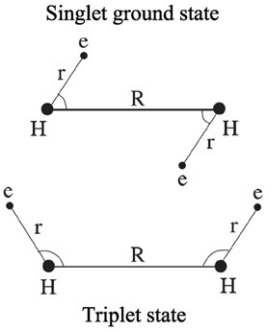

Figure 17. Bohr model electron configurations for the lowest singlet and triplet states of H_2 molecule.

$$g(r,R)=\int a(1)b(1)\frac{1}{r_{b1}}\mathrm{d}\mathbf{r}_1=\frac{1}{r}\exp\left(-\frac{R}{r}\right)\left(1+\frac{R}{r}\right),$$

$$S(r,R)=\int a(1)b(1)\mathrm{d}\mathbf{r}_1=\exp\left(-\frac{R}{r}\right)\left(1+\frac{R}{r}+\frac{R^2}{3r^2}\right).$$

When we apply the constrained Bohr model to H_2, the resulting energy function is

$$E(r,R)=\frac{1}{r^2}-\frac{2}{r}+2\Phi(r,R)+\frac{1}{r_{12}}+\frac{1}{R}. \tag{4.9}$$

This has an extremum when $r_{a1}=r_{b2}=r$ and $r_{a2}=r_{b1}$. Figure 17 shows the corresponding electron configurations for the ground singlet and triplet states; there, for the singlet state

$$r_{12}=\sqrt{2r^2-R^2+\frac{2}{\Phi^2(r,R)}},$$

and for the triplet state,

$$r_{12}=\frac{1}{R\Phi^2(r,R)}-\frac{r^2}{R}.$$

These are just geometric distances between the two electrons expressed in terms of R, r, and r_{b1}; the angle θ is determined by $\Phi^{-2}=R^2+r^2-2rR\cos\theta$.

Figure 18 shows, for both the singlet and triplet states, the potential energy curves, $E(R)$, obtained by minimization of the energy function, Equation (4.9), with respect to r. There are no fitting parameters in our calculations. Over the full range of R, the HM version (solid curves) and HL version (dotted curves) of the constrained Bohr model are remarkably close to the accurate curves (heavy dots). For the ground state singlet state, the bond dissociation energy obtained using the constraint potential is 4.99 eV from the HM version, 4.50 eV, from the HL, as compared with 4.745 eV from accurate results. (Since the Bohr model is not fully quantum mechanical, it is not subject to the variational principle, so need not give either an upper or lower bound.) The constrained Bohr model

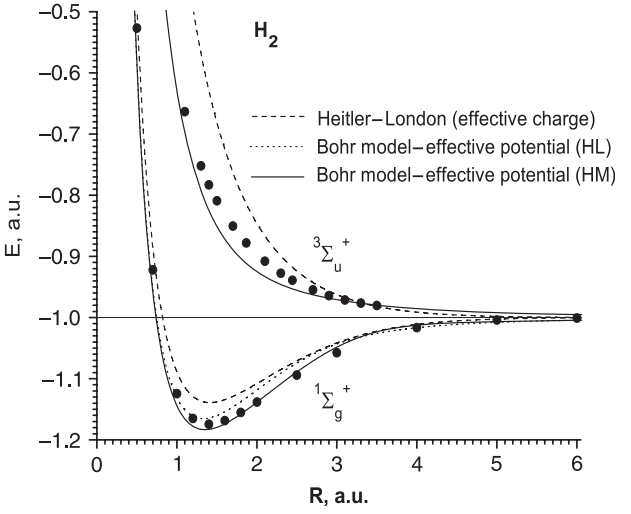

Figure 18. Potential energy curves for the ground $^1\Sigma_g^+$ and first triplet state $^3\Sigma_u^+$ of the H_2 molecule. Solid curves are obtained from the constrained Bohr model [81], using Φ_{HM} effective constraint potential, Equation (4.8), and dotted curves using Φ_{HL} version, Equation (4.7). Dashed curves are from HL variational treatment [82] with effective nuclear charge ($Z = 1.166$). Heavy dots show results from accurate calculations [36,37].

actually gives much better results than conventional wave mechanics using the HM or HL wavefunctions. The latter, even when enhanced by taking the nuclear charge as a variational parameter, give the H_2 bond strength as 3.43 eV from HM, 3.76 eV from HL. Conventional variational calculations for H_2 require wavefunctions with several adjustable parameters as well as configuration interaction, in order to attain accuracy over the full range of R comparable to that obtained from the constrained Bohr model.

Figure 19 presents an exploratory application of the constrained model to the first excited $^1\Sigma_g^+$ state of H_2 (labelled E by Herzberg [83]). This state is of particular interest because its potential energy curve has a double well structure. Such structures typically arise from 'avoided crossings' of zero-order potential curves corresponding to different electronic configurations. In a molecular orbital description for this state, at small R the configuration is $1s\sigma_g 2s\sigma_g$, at large R it becomes $\sigma_g 1s\sigma_g 2s$. The Bohr model exhibits distinct configurations, as seen in Figure 19: structure A at low R and B at large R. For the A configuration, the energy function is

$$E = \frac{1}{2r_1^2} + \frac{n^2}{2r_3^2} + V, \tag{4.10}$$

where $n = 2$ and the r_i distances are defined in Figure 19 (insert). Minimizing this function with the constraints

$$-\frac{1}{r_2} = \Phi_s(r_1, R), \qquad -\frac{1}{r_4} = \Phi_s(r_3, R)$$

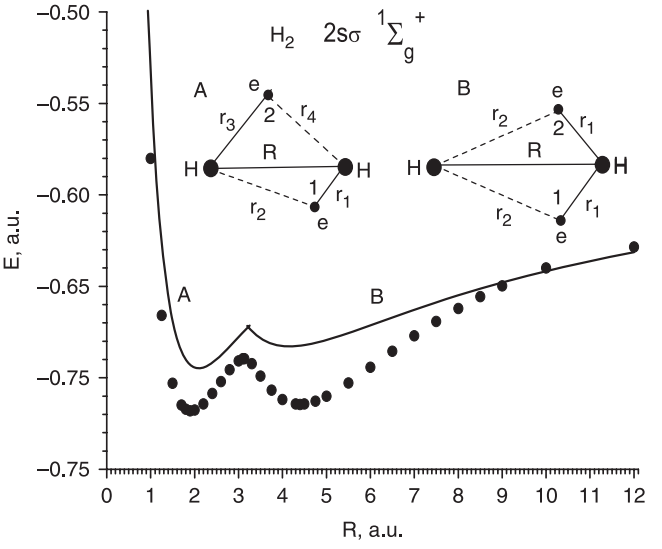

Figure 19. Potential energy curve for first excited state of H_2 with $^1\Sigma_g^+$ symmetry; solid curve obtained from constrained Bohr model [81], compared with heavy dots for accurate result [72]. Insert depicts Bohr electron configurations, A for small R and B for large R; the B configuration dissociates to H^+ and H^-.

yields the potential energy curve A plotted in Figure 19. For the B configuration, at large R the molecule separates into H^- and H^+ ions; the Bohr energy function is

$$E = \frac{1}{r_1^2} + \frac{n^2}{2r_2^2} + V, \tag{4.11}$$

with the constraint

$$-\frac{1}{r_2} = \Phi_s(r_1, R).$$

Note that the energy function of Equation (4.11), from which we obtain curve B of Figure 19, assumes quantization of both electrons relative to one of the nuclei with the principle quantum number equal to one. This quantization allows formation of the H^- ion. At the same time, one of the electrons is also quantized relative to the opposite nucleus with $n = 2$, a schizophrenic aspect exemplifying Bohr's favourite concept of complementarity. Combining curves A and B produces a double well structure fairly similar to that found in accurate calculations.

This result, for an excited state involving mixed configurations, encourages further exploration of the constraint approach. The constraints applied in this case are surely not optimal, as we merely used the Φ_{HL} function from Equation (4.7) derived for the singlet ground state rather than modifying the HL wavefunction.

4.2. *Application to H_3*

Generalizing the constraint approach to ground states of molecules comprising several hydrogen atoms is straightforward. If we consider electron 1 belonging to its nearest

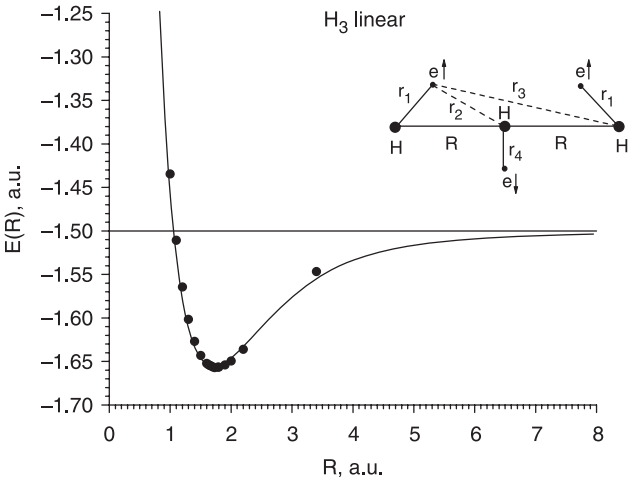

Figure 20. Potential energy function and Bohr electron configuration for symmetric stretching of linear H_3 molecule; solid curve obtained from constrained Bohr model [81], dots from accurate calculations [84,85].

nucleus and denote the distances from that electron to nuclei i as r_i ($i = 1, 2, \ldots$), then the constraint equation reads

$$-\sum_{i>1}\frac{1}{r_i} = \sum_{i>1}\Phi_i(r_1, R_i), \tag{4.12}$$

where R_i is the separation between the nucleus 1 and nucleus i. The mutual spin orientation of electrons 1 and i (belonging to the nucleus i) determines the choice of a singlet or triplet Φ_i in Equation (4.12).

In applying our model to the triatomic H_3 molecule, we consider symmetrical linear and triangular configurations, as shown in the inserts of Figures 20 and 21, with the spacing between adjacent nuclei the same, equal to R. For the linear case, the symmetry ensures that the Bohr model has the central electron at equal distances form the two neighbouring nuclei. For this electron, since its position is fixed, there is no collapse and thus no need for any constraint. As we only need to constrain the two outer electrons, Equation (4.12) reduces to

$$-\frac{1}{r_2}-\frac{1}{r_3} = \Phi_s(r_1, R) + \Phi_t(r_1, 2R), \tag{4.13}$$

where r_i are defined in the insert of Figure 20. Adjacent electrons in the linear ground state have opposite spins, so require a singlet constraint potential. As the two outer electrons have parallel spins, they require a triplet constraint. The Bohr energy function

$$E = \frac{1}{r_1^2} + \frac{1}{2r_4^2} + V \tag{4.14}$$

was minimized subject to Equation (4.13), using the HM version of the constraint functions. As seen in Figure 20, this gave a potential energy curve in excellent agreement with the accurate results.

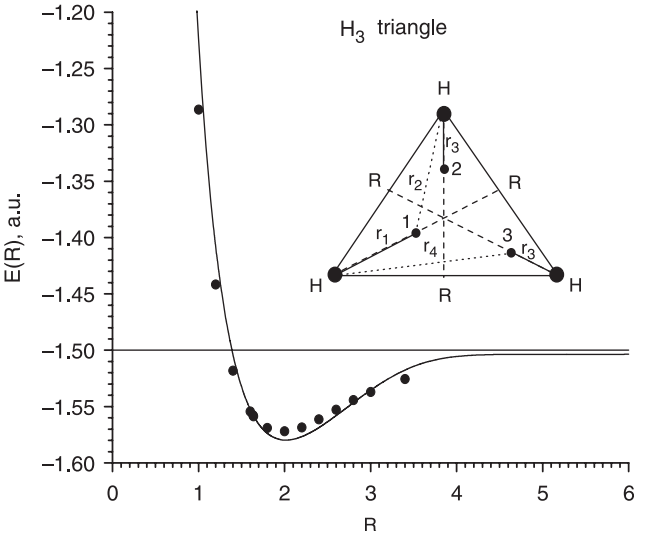

Figure 21. Potential energy function and Bohr electron configuration for symmetric breathing motion of equilateral triangular H_3 molecule; solid curve obtained from constrained Bohr model [81], dots from accurate calculations [84,85].

For the triangular case, we assume that electron 1 has spin opposite to those of electrons 2 and 3. Symmetry dictates that electron 1 lies above the plane of the nuclei, while electrons 2 and 3 lie below. Also, the projections on the plane of the positions of all three electrons lie along bisectors of the equilateral triangle. Thus, the constraint potential of Equation (4.12) for electron 1 reads

$$-\frac{1}{r_2} = \Phi_s(r_1, R), \tag{4.15}$$

while that for electrons 2 and 3 reads

$$-\frac{2}{r_4} = \Phi_s(r_3, R) + \Phi_t(r_3, R). \tag{4.16}$$

Minimization of the Bohr model energy function

$$E = \frac{1}{2r_1^2} + \frac{1}{r_3^2} + V \tag{4.17}$$

subject to these constraints again yields, as seen in Figure 21, a potential energy curve in very good agreement with accurate results over the full range of R.

5. *D*-scaling transformations: link to Bohr model

In relating the Bohr model to the large-D limit of the Schrödinger equation in Section 2, we introduced a D-dependent length scale and also incorporated into the probability distribution a D-dependent portion of the Jacobian factor. Here we consider the D-scaling

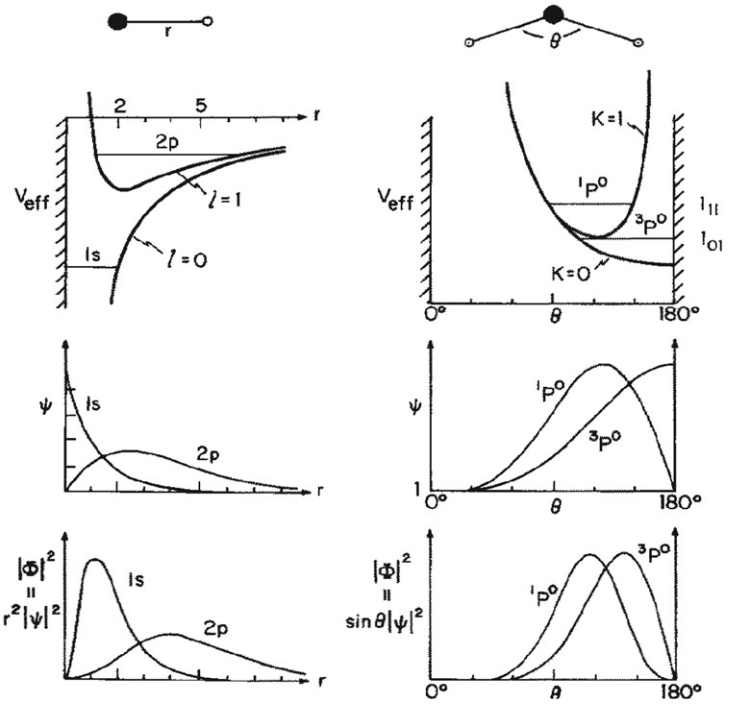

Figure 22. Role of Jacobian volume element, illustrated for H atom and for model problem of two electrons on a rigid sphere. Effective potentials have infinite barriers (at $r=0$ and at $\theta=0^\circ$ and 180°) corresponding to points at which the Jacobian vanishes. At such points, the wavefunction ψ for some states ($l=0$ or $K=0$) can have maxima, but the corresponding Jacobian-weighted probability density $|\Phi|^2$ must vanish. Taken from [86].

procedure more closely, to provide a broader context for the Bohr model and to point out generic aspects and important variants that may foster further developments.

As a prelude, in Figure 22 we note a pair of simple examples. Typical textbooks lead up to the Bohr H atom by pointing out that classical mechanics would allow the electron to spiral into the nucleus. Students are then confused (or should be!) to read a few pages later that the ground state $1s$ wavefunction peaks at $r=0$. Doesn't that mean the electron is most likely to be found at the nucleus? No! The instructor should make clear that in curvilinear coordinates account must be taken of the non-uniform weighting of space introduced by the Jacobian volume element, J. To evaluate the most probable geometry requires a transformation to a new probability amplitude, $\Phi = J^{1/2}\Psi$. The transformed amplitude must vanish wherever J does, since Ψ is finite everywhere. For the H atom in any s-state, the radial wavefunction Ψ does have its maximum at the origin, but $|\Phi|^2 = r^2|\Psi|^2$ vanishes there and for the ground state has its maximum at the Bohr radius.

A kindred example, concerning electron distribution in the ground state of He ($1s^2\ ^1S$), has confused many professional chemists and physicists. They happily assert that the most probable location of the two electrons has them 180° apart. Actually, the most probable interelectron angle is $\sim 95^\circ$. This is just an angular analog to the H atom radial case. The essential aspect is shown in Figure 22, for the model problem of two electrons moving

on a rigid sphere [86]. The Ψ for the $K=0$ state peaks at 180°, but the probability density $|\Phi|^2=\sin\theta|\Psi|^2$ vanishes there and has its maximum at a much lower angle. The He atom ground state is likewise 'bent'.

Such consequences of Jacobian weightings may appear counterintuitive, but only if attention is restricted to electrostatics. In He, the Coulombic repulsion does want the electrons to be 180° apart, just as in the H atom Coulombic attraction impels the electron to the nucleus. In both cases, the most probable geometry is actually governed by the uncertainty principle, which induces zero-point kinetic energy that resists the electrostatic preference. The shape as well as the size of atoms stems from quantum duality.

In D-scaling, the Jacobian weighting and its D-dependence has a prominent role, examined further below as it becomes especially important when dealing with geometric aspects of the Bohr model.

5.1. *Interplay of Laplacians and Jacobians*

The first step in D-scaling is to generalize the Schrödinger equation to D-dimensions. This involves transforming the Laplacian operator and Jacobian volume element, from a Cartesian space in which all vectors are endowed with D components, into appropriate curvilinear coordinates. The potential energy retains its $D=3$ form.

Hyperspherical coordinates are the natural choice for atoms. The coordinate transformation has a nested structure:

$$\begin{aligned}
x_1 &= r\cos\theta_1 \sin\theta_2 \sin\theta_3 \cdots \sin\theta_{D-1},\\
x_2 &= r\sin\theta_1 \sin\theta_2 \sin\theta_3 \cdots \sin\theta_{D-1},\\
x_3 &= r\cos\theta_2 \sin\theta_3 \sin\theta_4 \cdots \sin\theta_{D-1},\\
x_4 &= r\cos\theta_3 \sin\theta_4 \sin\theta_5 \cdots \sin\theta_{D-1},\\
&\vdots \quad \vdots\\
x_j &= r\cos\theta_{j-1} \sin\theta_j \sin\theta_{j+1} \cdots \sin\theta_{D-1},\\
&\vdots \quad \vdots\\
x_{D-1} &= r\cos\theta_{D-2} \sin\theta_{D-1},\\
x_D &= r\cos\theta_{D-1},
\end{aligned} \tag{5.1}$$

$$r\geq 0, \quad \theta_0=0, \quad 0\leq\theta_1\leq 2\pi, \quad 0\leq\theta_j\leq\pi \quad \text{for} \quad j=2,3,\ldots,D-1,$$

where D is a positive integer and $D\geq 2$. The resulting Laplacian has the form

$$\nabla_D^2 = K_{D-1}(r) - \frac{L_{D-1}^2}{r^2}, \tag{5.2}$$

where

$$K_{D-1}(r) \equiv \frac{1}{r^{D-1}}\frac{\partial}{\partial r}\left(r^{D-1}\frac{\partial}{\partial r}\right). \tag{5.3}$$

and the generalized angular momentum operator L^2_{D-1} is defined recursively by

$$\begin{aligned} L_1^2 &= -\frac{\partial^2}{\partial\theta_1^2}, \\ L_2^2 &= -\frac{1}{\sin\theta_2}\frac{\partial}{\partial\theta_2}\sin\theta_2\frac{\partial}{\partial\theta_2} + \frac{L_1^2}{\sin^2\theta_2}, \\ &\vdots \quad \vdots \\ L_k^2 &= -\frac{1}{\sin^{k-1}\theta_k}\frac{\partial}{\partial\theta_k}\sin^{k-1}\theta_k\frac{\partial}{\partial\theta_k} + \frac{L_{k-1}^2}{\sin^2\theta_k}. \end{aligned} \tag{5.4}$$

This Laplacian was obtained more than a century ago [87]; detailed derivations are readily available [14,88–91].

For a single particle subject to a central force potential, $V(r)$, the Schrödinger equation is

$$\left(-\frac{1}{2}\nabla_D^2 + V(r)\right)\Psi_D = E\Psi_D. \tag{5.5}$$

By virtue of the spherical symmetry, the radial and angular dependence may be separated by

$$\Psi_D(r, \Omega_{D-1}) = R_D(r)\,Y(\Omega_{D-1}), \tag{5.6}$$

where the angular factor, a hyperspherical harmonic [92], is an angular momentum eigenfunction,

$$L^2_{D-1}\,Y(\Omega_{D-1}) = C\,Y(\Omega_{D-1}), \tag{5.7}$$

and C is the eigenvalue, to be determined. When evaluating $Y(\Omega_{D-1})$, we can fix r at any non-zero value and chose any convenient magnitude for $V(r)$; thus by setting $V(r) = E_D$, we reduce Equation (5.5) to the Laplace equation, $\nabla_D^2\Psi_D = 0$. Since near the origin ($r = 0$), $\Psi_D \sim r^\ell\,Y(\Omega_{D-1})$, we find

$$\nabla_D^2\left[r^\ell\,Y(\Omega_{D-1})\right] = [\ell(\ell + D - 2) - C]r^{\ell-2}\,Y(\Omega_{D-1}) = 0, \tag{5.8}$$

and thus $C = \ell(\ell + D - 2)$, with $\ell = 0, 1, 2, \ldots$. The radial part of the Hamiltonian therefore is given by

$$H_D = -\frac{1}{2}K_{D-1}(r) + \frac{\ell(\ell + D - 2)}{2r^2} + V(r). \tag{5.9}$$

This is simplified further by $\Phi_D = r^{(D-1)/2}R_D(r)$, incorporating the square root of the radial part of the Jacobian factor, $J_D = r^{D-1}\sin^{D-2}\theta$. The corresponding equation for the probability amplitude is

$$\left[-\frac{1}{2}\frac{\partial^2}{\partial r^2} + \frac{\Lambda(\Lambda + 1)}{2r^2} + V(r)\right]\Phi_D = E_D\Phi_D, \tag{5.10}$$

where

$$\Lambda = \ell + \frac{1}{2}(D - 3). \tag{5.11}$$

The net result, for any central force potential, is seen to have the same form as that for $D=3$, but in the centrifugal term the orbital angular momentum of Equation (5.10) has acquired a D-dependent increment. There is thus an *inter-dimensional degeneracy*: an increase in the spatial dimension by two ($D \to D+2$) is equivalent to adding one quantum of orbital angular momentum [93].

For the H atom, with $V(r)=1/r$, the contribution of orbital momentum results in increasing the principal quantum number by the same increment,

$$n \to n + (D-3)/2. \tag{5.12}$$

By use of these transcriptions for n and ℓ, all properties of the H atom in D-dimensions can be obtained simply from those for $D=3$.

For two-electron atoms such as He, in S states the D-dimensional Hamiltonian can be set-up in a fashion analogous to that for the H atom. It likewise can be cast in the same form as that for $D=3$, with the addition of a scalar centrifugal potential which contains the sole dependence on D as a quadratic polynomial. This is a key theorem, valid for S states of any N-body system [94]. For helium-like atoms, the S-state wavefunction depends only on the electron–nucleus radii r_1 and r_2 and the angle θ between these radii. Table 1 summarizes results for the Laplacian and kindred quantities. Note that among the $D-1$ angles on which the angular momentum operator L^2_{D-1} depends, only θ is non-separable, since it is the only angle that appears in the kinetic and potential energy. Hence, L^2_{D-2} will be a constant of the motion and so can be replaced by its eigenvalue, $L(L+D-3)$, which vanishes for S-states.

If the probability amplitude is defined by $\Phi_D = J_D^{1/2}\Psi_D$, incorporating the full Jacobian factor, the corresponding Schrödinger equation is

$$(T+U+V)\Phi_D = E_D\Phi_D, \tag{5.13}$$

where derivatives appear only in

$$T = -\frac{1}{2}\left[\frac{\partial^2}{\partial r_1^2} + \frac{\partial^2}{\partial r_2^2} + \left(\frac{1}{r_1^2}+\frac{1}{r_2^2}\right)\frac{\partial^2}{\partial\theta^2}\right]. \tag{5.14}$$

Because, by construction, the Jacobian associated with this Φ_D is simply unity, T takes a quasi-Cartesian form, so contains only second derivatives. The centrifugal term U is given in Table 1. The potential V contains the familiar Coulombic electron–nucleus

Table 1. Dimension dependent terms for H and He. All quantities in atomic units, with distances in Bohr units, energies in hartree.

Quantity	H atom	He atom, S states
∇_D^2	$K_{D-1}(r) - (L^2_{D-1})/r^2$	$\sum_i \left(K_{D-1}(r_i) - \frac{L^2_{D-1}}{r_i^2}\right)$
L^2_{D-1}	$\ell(\ell+\mathrm{D}-2)$	$-\frac{1}{\sin^{D-2}\theta}\frac{\partial}{\partial\theta}(\sin^{D-2}\theta)\frac{\partial}{\partial\theta} + \frac{L^2_{D-2}}{\sin^2\theta}$
J_D	$r^{D-1}\sin^{D-2}\theta$	$(r_1 r_2)^{D-1}\sin^{D-2}\theta$
U	$\frac{\Lambda(\Lambda+1)}{2r^2}$	$\frac{1}{2}\left(\frac{1}{r_1^2}+\frac{1}{r_2^2}\right)\left[-\frac{1}{4}+\frac{\Lambda(\Lambda+1)}{\sin^2\theta}\right]$
Λ	$\ell+\frac{D-3}{2}$	$\frac{D-4}{2}$

attraction and electron–electron repulsion. This form, although unconventional for electronic structure studies, is customary in molecular spectroscopy (with $U+V$ replaced by a vibrational potential).

Another convenient form for the Schrödinger equation can be obtained [94] by factoring the Jacobian as $J_D = J_3 J_{D-3}$, so that

$$J_3 = r_1^2 r_2^2 \sin\theta \text{ and } J_{D-3} = (r_1 r_2 \sin\theta)^{D-3}. \tag{5.15}$$

Then the transformation $\Psi_D = J_{D-3}^{-1/2}\Phi_D$ yields again Equation (5.13), but the derivative terms become

$$T = -\frac{1}{2}\left[K_2(r_1) + K_2(r_2) + L_2^2(\theta)\right], \tag{5.16}$$

and the centrifugal term becomes

$$U = \frac{1}{2}\left(\frac{1}{r_1^2} + \frac{1}{r_2^2}\right)\left(\frac{D-3}{2}\right)^2 \frac{1}{\sin^2\theta}. \tag{5.17}$$

The Schrödinger equation thus is the same as for $D=3$, except for the addition of the D-dependent centrifugal potential, and now the Jacobian for the $|\Phi_D|^2$ function is J_3. This is the preferred form for calculations employing conventional variational methods. It allows any existing computer code to be extended to D dimensions simply by adding the matrix elements for the centrifugal potential of Equation (5.17).

In general, a transformation $\Psi_D = \chi\Phi_D$, recasts the Laplacian via $\chi^{-1}\nabla^2\chi$, giving a Schrödinger equation like Equation (5.13) but altering the form of T and U as well as the Jacobian associated with the probability amplitude. In this context, the choice that led to the Bohr model, as presented in Section 2.1, is unorthodox but remarkably efficient. It takes $\chi = J_r^{-1/2}$ with J_r merely the radial portion of the Jacobian and retains the $D=3$ form for the angular portions of both the Laplacian and Jacobian. This fulfills the usual objectives of simplifying $\nabla^2\Phi_D$ and rendering the Jacobian associated with Φ_D independent of D. Moreover, it confines the explicit D-dependence of the Hamiltonian to the centrifugal term, which takes on the simple Bohr form

$$U(r_1, r_2) = \frac{1}{2}\left(\frac{1}{r_1^2} + \frac{1}{r_2^2}\right)\left(\Lambda + \frac{1}{2}\right)\left(\Lambda + \frac{3}{2}\right), \tag{5.18}$$

for the He S-states, with $\Lambda = (D-4)/2$, and thereby is freed from the awkward $1/\sin^2\theta$ factor (cf. Table 1). However, as discussed in Section 5.3, this has an important consequence, presaged in Figure 22. The large-D limit obtained by minimizing $U+V$ using Equation (5.18) will give $\theta_m = 180°$; to obtain a θ_m that approximates the $D=3$ interelectron angle, it is necessary to include in the χ-transformation the angular portion of the Jacobian.

Hypercylindrical coordinates are a natural choice for diatomic molecules [35]. These comprise a linear coordinate z orthogonal to a $(D-1)$ subspace. The subspace is specified by spherical coordinates: ρ, the radius of the $(D-1)$ hypersphere, and Ω_{D-2}, a set of $(D-2)$ angles. The coordinate transformation thus is nearly like Equation (5.1), except that $x_1 \to z$ and $r \to \rho$ while in the angle indices $(D-1) \to (D-2)$. Table 2 summarizes

Table 2. D-dependent terms for H_2^+ and H_2. All quantities in atomic units, with distances in Bohr units, energies in hartree.

Quantity	H_2^+ molecule	H_2 molecule, Σ states
∇_D^2	$K_{D-2}(\rho)+\frac{\partial^2}{\partial z^2}-\frac{L_{D-2}^2}{\rho^2}$	$\sum_i\left(K_{D-2}(\rho_i)+\frac{\partial^2}{\partial z_i^2}\right)-\left(\frac{1}{\rho_1^2}+\frac{1}{\rho_2^2}\right)L_{D-2}^2$
L_{D-2}^2	$\lvert m\rvert(\lvert m\rvert+D-3)$	$\frac{1}{\sin^{D-3}\phi}\frac{\partial}{\partial\phi}\left(\sin^{D-3}\phi\,\frac{\partial}{\partial\phi}\right)-\frac{L_{D-3}^2}{\sin^2\phi}$
J_D	$\rho^{D-2}(\sin\phi)^{D-3}$	$(\rho_1\rho_2)^{D-2}(\sin\phi)^{D-3}$
U	$\frac{\Lambda(\Lambda+1)}{2\rho^2}$	$\frac{1}{2}\left(\frac{1}{\rho_1^2}+\frac{1}{\rho_2^2}\right)\left[-\frac{1}{4}+\frac{\Lambda(\Lambda+1)}{\sin^2\phi}\right]$
Λ	$\lvert m\rvert+\frac{D-4}{2}$	$\lvert m\rvert+\frac{D-5}{2}$

the Laplacian and other D-dependent quantities for the one- and two-electron homopolar diatomics H_2^+ and H_2. The format enables easy comparison with those for H and He atoms in Table 1. For the molecules, the nuclei are located on the z-axis at $-R/2$ and $+R/2$, respectively. In H_2^+ the Coulombic interactions depend only on R and (ρ, z), the pair of coordinates that locate the lone electron. In H_2, the interaction involves five electronic coordinates: (ρ_1, z_1) and (ρ_2, z_2) and the dihedral angle ϕ between the pair of planes that contain the electrons and the molecular axis. The angular momentum operator L_{D-2}^2 can be replaced by its eigenvalue in the case of H_2^+, since all of the $D-2$ angles are separable, including the azimuthal angle ϕ which exists for $D=3$. The corresponding quantum number, denoted by $|m|=0,1,2,\ldots$, is the magnitude of the projection of the orbital angular momentum on the linear axis z. The L_{D-2}^2 operator is not a constant of motion in the case of H_2, since the dihedral angle ϕ is not separable. The other angles are all separable, however. As with the He atom, we need only step down by $D\to D-1$ to reach an operator that is constant, namely L_{D-3}^2, with eigenvalue $|m|(|m|+D-4)$.

Included in Table 2 are the expressions for the centrifugal potentials obtained by incorporating the square root of the full Jacobian into the probability amplitude. Our discussion above of variants that arise when less than the full Jacobian is used applies as well to molecules. In particular, for H_2, if only the radial Jacobian factor is tucked into Φ_D, the Bohr model expression for $U(\rho_1, \rho_2)$ is obtained. Analogous to Equation (5.18), it again depends quadratically on D but is independent of the dihedral angle. Comparison of Table 2 with Table 1 exhibits correspondences with the united atoms ($H_2^+\to He^+$, $H_2\to He$), including systematic aspects of switching between spherical and cylindrical coordinates.

Hartree–Fock version since the correlation energy is defined as the error in the Hartree–Fock (HF) approximation, it is often of interest to compare D-scaling results with the HF version [95,96]. As with the analogous mean field approximation in statistical mechanics, the error in a HF treatment is expected to diminish as D increases. This is because fluctuations decrease in proportion to $D^{-1/2}$, as readily shown for the H atom. However, whereas the mean field approximation for critical exponents of phase transitions becomes exact for sufficiently large D, for the HF approximation the correlation energy (CE) remains non-zero and relatively large even for $D\to\infty$. As a fraction of the total energy, the CE for the He atom varies from 2.3% at the $D\to 1$ limit to 1.5% for $D=3$ to 0.99% at the $D\to\infty$ limit.

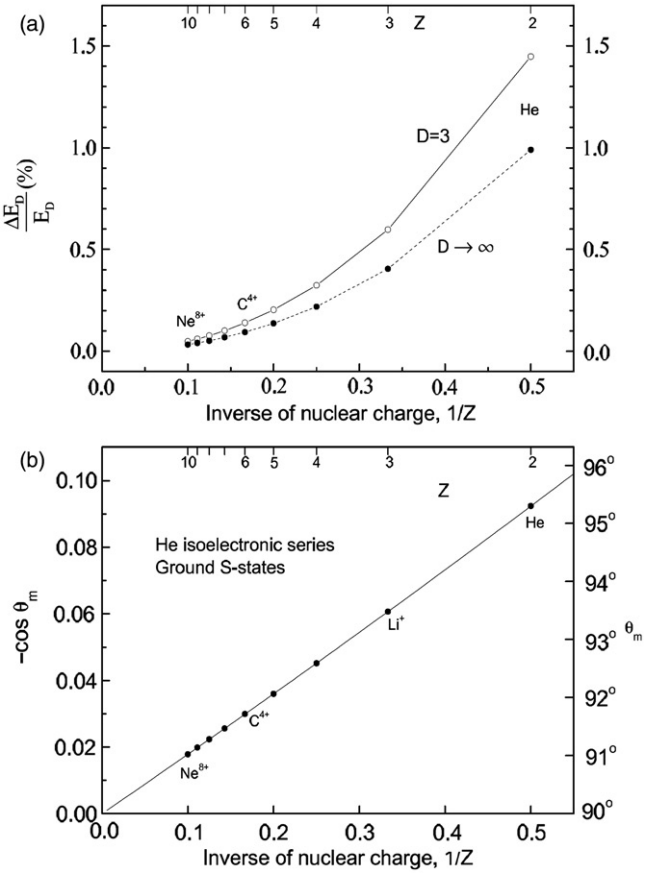

Figure 23. For two-electron atom ground states, variation with reciprocal of nuclear charge, $1/Z$, of (a) cosine of most probable interelectron angle θ_m for large-D limit and (b) correlation energy ΔE_D for $D=3$ and $D\to\infty$, as a percentage of the total electronic energy.

The origin of this residual HF error at the large-D limit is another Jacobian effect. The HF wavefunction, constructed as a product of one-electron orbitals, lacks any explicit dependence on the angle between the electron radii. Hence this angle enters only in the Jacobian volume element, which contains $\sin^{D-2}\theta$ in hyperspherical coordinates and $\sin^{D-3}\phi$ in hypercylindical coordinates. Therefore, as $D\to\infty$, the angle becomes fixed at 90°. That constraint does not allow the HF method to find the correct minimum of the effective potential, $U+V$, at the large-D limit. For instance, this limit for the ground state of He has $\theta_m=95.3°$; the deviation from 90° is a direct measure of the correlation energy.

Figure 23 displays the variation of $\cos\theta_m$ and the correlation energy with $1/Z$ for the ground S states of two-electron atoms. The interelectron angle, found by minimizing $U+V$ at the large-D limit [18,97–99], is given by

$$-\cos\theta_m = x^2 + x(x^2+2)^{1/2} = 2^{-5/2}\lambda + 2^{-6}\lambda^2 + \cdots, \tag{5.19}$$

with $x = \lambda/8$ and $\lambda = 1/Z$. Expansions in λ for the correlation energy, $\Delta E_D = E_D - E_D^{\mathrm{HF}}$, are given in [100]. As Z increases, θ_m moves closer to 90°, and the correlation energy decreases, reflecting the diminishing importance of electron–electron repulsion relative to attraction of the electrons to the nucleus.

5.2. *Variant scalings to tame D-singularities*

The next, key step is to transform to a suitably scaled space to remove the major, generic D-dependence of the quantity to be determined. Usually the scaled quantity can be evaluated at one or more special D-values, such as $D \to \infty$, where the computation is often easy. Then an approximation for $D = 3$ can be obtained by relating it to the special D-value(s).

Here we consider chiefly electronic energies. The hydrogen atom again serves as a guide [14,101,102]. By means of the transcription provided by Equation (5.12), we find that in D-dimensions the ground state ($n = 1, l = 0$) wavefunction and energy are

$$\Psi_{\mathrm{o}}(r) = \exp\left(-\frac{2r}{D-1}\right), \quad E_{\mathrm{o}} = -\frac{2}{(D-1)^2}. \tag{5.20}$$

The D-dependence is drastic: when $D \to 1$ the atom implodes and when $D \to \infty$ it falls apart. Between these limits, as D is decreased, the atom shrinks in size and binds its electron more tightly, whereas as D is increased, the atom expands and loosens its electron. We want to remove or moderate the D-dependence by introducing distance and energy scalings, chosen to have no effect at $D = 3$.

As seen above, the centrifugal portion of the Laplacian grows quadratically with D, so pushes the atom apart. Hence, in general, the scaling needs to divide Laplacians by factors quadratic in D, equivalent to scaling r as D^2 as $D \to \infty$, in order to obtain a finite limit. In contrast, at low D the attractive Coulomb terms collapse the atom because they are no longer inhibited by centrifugal barriers. To tame the $D \to 1$ singularity thus requires multiplication by $(D-1)$, which gives

$$\lim_{D\to 1} \frac{D-1}{2r} = \delta(r), \tag{5.21}$$

and the delta function potential yields a finite ground state energy.

Most often, the scalings needed to render the low-D and large-D limits finite have been considered independently of each other. The commonly used version termed *hydrogenic scaling* takes the distance unit proportional to the *square* of $\kappa = (D-1)/2$ in dealing with the large-D regime, but instead takes the distance unit *linear* in κ when treating the low-D region. For applications to atoms, this inconsistency does not matter when computing the energy (proportional to κ^{-2} in both regimes), since that involves averages over the electronic coordinates and the scaling factors for distance then cancel out.

However, in treating properties of atoms or molecules that involve a length scale that is not integrated out, we need a different scaling scheme. The simplest molecule, H_2^+, exemplifies this. In the Born–Oppenheimer approximation, the electronic energy depends parametrically on the internuclear distance, R. Use of hydrogenic scaling, which scales R differently for the $D \to \infty$ and $D \to 1$ limits, makes the electronic energy curves $E_D(R)$ incommensurate in those limits. An unwelcome consequence became apparent in a study of H_2^+ and H_2 molecules that used the same hydrogenic scaling employed for atoms [35].

With that scaling, the united atom ($R \to 0$: He^+) and separated atom ($R \to \infty$: $H + H^+$) limits are both correct. Also, the electronic energy for $D \to \infty$, determined as usual from the global minimum of the centrifugal plus Coulombic terms, but without the nuclear repulsion ($1/R$) term, varies smoothly between these limits. However, when the nuclear repulsion is added, to obtain the molecular potential energy curve, $E(R)$, the net interaction is repulsive. Thus, at least with hydrogenic scaling, for these molecules the combined effect of the centrifugal and nuclear repulsion precludes chemical bonding as $D \to \infty$.

A simple cure is provided by adopting a procedure termed *uniform scaling*, proposed by Loeser [101,102]. This retains the energy scaling as κ^{-2}, but makes the distance unit proportional to $D(D-1)/6$ for all D. This distance scale factor interpolates smoothly between the hydrogenic dependence, proportional to D^2 at large-D and to $(D-1)$ at low-D, and reduces to unity at $D=3$. As well as reconciling the dimensional limits, use of uniform scaling brings a major part of the chemical bonding contributions into both the large-D and low-D limits.

Figure 24 illustrates for H_2^+ the taming of D-dependence provided by uniform scaling [14]. The unscaled internuclear distance R is related to R_H and R_U, the large-D hydrogenic and the uniform scaled versions, by

$$R = \left(\frac{D-1}{2}\right)^2 R_H = \frac{D(D-1)}{6} R_U. \tag{5.22}$$

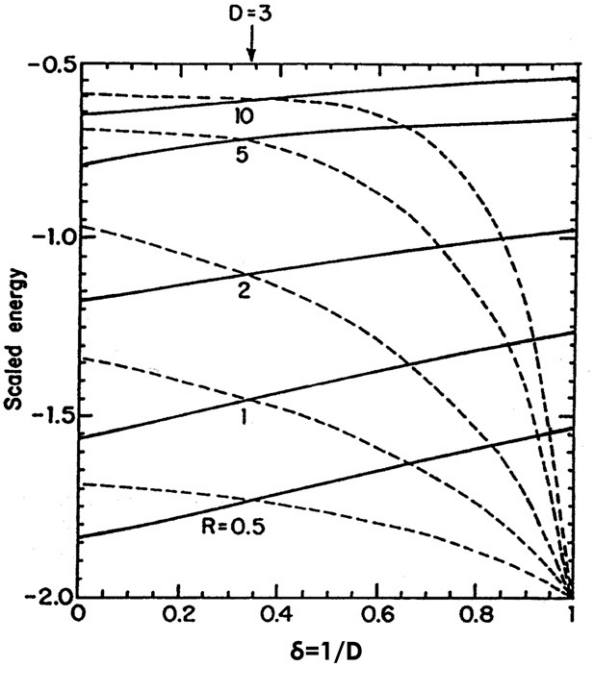

Figure 24. Electronic energy of ground-state H_2^+ (in units of κ^{-2} hartrees) as a function of $\delta = 1/D$ for fixed values of scaled internuclear distance, R_H (dashed curves) or R_U (solid curves), defined in Equation (5.22). For $D=3$, the scalings reduce to unity; thus curves are labelled simply by unscaled R (bohr units). From [14].

The energy E_D as a function of R_H (shown as dashed curves) varies strongly with $\delta = 1/D$. In particular, as $D \to 1$ the energy descends to the united atom limit ($R \to 0$) for all values of R_H. This does not happen when the energy is expressed instead as a function of R_U (solid curves) because the uniform scaling incorporates the correct limiting behaviour. With uniform scaling, the electronic energy also lies lower at the $D \to \infty$ limit. This offsets enough of the nuclear repulsion to enable the large-D limit to provide a qualitatively good approximation to the molecular potential energy curve [35]. Also, $E_D(R_U)$ becomes approximately linear in $1/D$, thereby facilitating dimensional interpolation.

Figure 25 shows potential curves obtained for H_2^+ by adding the nuclear repulsion, $1/R$, to the electronic energies evaluated with uniform scaling for the $D \to 1$ (dotted) and $D \to \infty$ (dashed) limits; both now exhibit bonding. Also shown is the approximation for $D = 3$ (dot-dashed) provided by interpolating linearly in $1/D$ between the limits via

$$E_3(R) \approx \frac{1}{3} E_1^u(R) + \frac{2}{3} E_\infty^u(R). \tag{5.23}$$

This blithe interpolation comes close to the accurate $D = 3$ results (heavy dots), for both the bond dissociation energy and bond length. Further analysis finds that for H_2^+ near its equilibrium bond length, the dimension dependence of the ground-state electronic energy is dominated by the singularities at $D \to 1$, congruent second and first order poles. These poles are generic for Coulombic potentials, as they result from particle coalescences. Other examples likewise confirm the inference from H_2^+ of the virtue of incorporating these low-D features in a commensurate way, as accomplished by uniform scaling.

Another drawback of the hydrogenic scaling originally used is that the energy expressions obtained for excited atomic states collapsed to the ground state as $D \to \infty$.

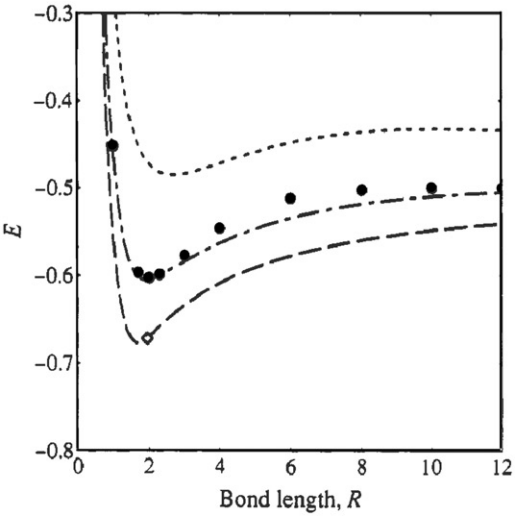

Figure 25. Dimension interpolation for H_2^+. Plotted are $D \to 1$ (dotted curve) and $D \to \infty$ limit (dashed curve), the interpolated values (dot-dashed) obtained from Equation (5.23) and heavy dots from accurate $D = 3$ calculations. Diamond on large-D limit curve marks symmetry breaking point; for $R > (9/8)\sqrt{3}$ the electron lies off-centre. Taken from [101,102].

The cure for this, as shown by van der Merve [97–99], is to introduce semiclassical quantization into the large-D limit. That supplies the appropriate principal quantum numbers, n_i, as in Equation (2.12), and thus ensures that the energies correspond to excited states. We consider another way to do this in Section 6.

5.3. *Bohr model contrasted with other large-D limits*

The perspective offered by our discussion of basic D-scaling makes more striking the effectiveness of the Bohr model. Its use of just hydrogenic rather than uniform scaling would be expected to handicap treatment of chemical bonding. Yet, for H_2 that evidently is offset by its unorthodox suppression of the $1/\sin^2\phi$ angular factor in U, the centrifugal term (Table 2). As noted in Section 2, the angular dependence of U fosters interelectron angles near 90°. That competes with the Coulombic potential V, wherein electron–electron repulsion fosters angles approaching 180°. In the Bohr model, omission of the angular portion of the Jacobian weighting allows $\phi_m = 180°$, minimizing the $1/r_{12}$ electron–electron repulsion, and thereby contributes to chemical bonding.

In contrast, the orthodox large-D treatment, which includes the full Jacobian weighting, has the $1/\sin^2\phi$ factor in U and the $\sin^{D-3}\phi$ factor in the Jacobian strongly shifts ϕ_m towards 90°. This enhances, indeed much overweights, the $1/r_{12}$ repulsion and thereby inhibits chemical bonding. Thus, as seen in Sections 2 and 3, the Bohr model variant of D-scaling, which retains the $D = 3$ form of the angular portion of the Jacobian and Laplacian, enables the large-D limit to provide a much better zero-order approximation for H_2 at $D = 3$ than does the orthodox 'Full-J' scaling.

However, for the He atom the Bohr variant suffers from a major disadvantage, exhibited in Table 3. In the large-D limit Bohr scaling makes the interelectron angle

Table 3. Energy and geometry for He ground state.

Method	$-E_m$ (a.u.)	r_m (a_0)	θ_m (°)
$D \to \infty$ limit			
'Full-J'	2.7378	0.6069	95.3
Hartree–Fock	2.7108	0.6074	90.0
Bohr Model	3.0625	0.5714	180.0
$D = 3$ results			
Tatum[1]	2.9037	0.60	94.6
Pekeris[2]	2.9037	0.620	94.3
CH[3]	2.9037	0.6047	100.0
Chin[4]	2.878	0.5791	97.8
Hartree–Fock[5]	2.8617	0.569	90.0

[1]From [103], where a 39-term Hylleraas wavefunction was used. Note: as *ab initio* calculations do not customarily report the most probable interelectron angle θ_m, we have derived nominal values either via $\theta_m = \cos^{-1}\langle\cos\theta\rangle$ or from other expectation values. As θ_m is somewhat sensitive to the shape of the angular distribution, the nominal values may be uncertain by several degrees.
[2]From [104]; angle calculated from $\theta_m \sim \cos^{-1}(\langle \mathbf{r_1}\cdot\mathbf{r_2}\rangle/\langle r_1\rangle^2)$.
[3]From [105], where an 18-term wavefunction was used.
[4]From [106], which used a 2-term wavefunction.
[5]Wavefunction and energy taken from [53].

$\theta_m = 180^\circ$ for the ground S-state, whereas 'Full-J' scaling gives $\theta_m = 95.3^\circ$, close to the result from high-quality *ab initio* calculations for the $D = 3$ atom. This consequence of the choice of Jacobian weighting, anticipated in Figure 22, is illustrated further with contour maps displayed in Figure 26 for a modest $D = 3$ variational wavefunction [106]. The Bohr model result indeed corresponds to the crest of the wavefunction, Ψ; but the most probable value of θ corresponds to the maximum of the probability amplitude, $|\Phi|^2 = J|\Psi|^2$, which for $D = 3$ is proportional to $\sin\theta|\Psi|^2$.

These comparisons suggest a simple rule. To select a scaling which enables the simple large-D limit to provide a good approximation for $D = 3$, be guided by the form of the $D = 3$ Jacobian. For H_2, since $J_3 = \rho_1\rho_2$ has no angle dependence, use a scaling that does not include the angular part of $J_D \sim \sin^{D-3}\phi$. For He, since $J_3 = r_1^2 r_2^2 \sin\theta$ does have angle dependence, use a scaling that does include the angular part of the Jacobian, $J_D \sim \sin^{D-2}\theta$. This also suggests that improvements may be sought by taking the liberty

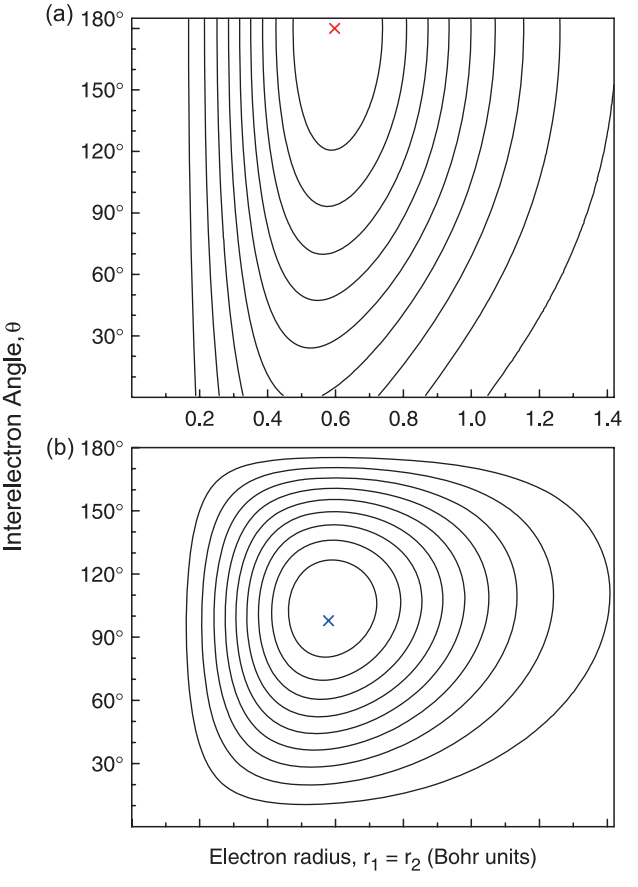

Figure 26. Contour maps of Jacobian weighted density. (a) Bohr model weighting, $r_1^2 r_2^2|\Psi|^2$; cross indicates the most probable radii and angle $r_m^B = 0.5973$, $\theta_m^B = 180^\circ$. (b) Full Jacobian result, $r_1^2 r_2^2 \sin\theta|\Psi|^2$; cross indicates the most probable radii and angle $r_m^F = 0.5791$, $\theta_m^F = 97.85^\circ$. The Ψ used is from [106].

to modify the Jacobian. We consider a step in that direction in Section 6 and discuss other prospects in Section 8.

6. Quantum-number *D*-scaling for multielectron atoms

A straightforward D-scaling approach for excited electronic states of atoms associates them with vibrational and rotational modes of the electrons with respect to the frozen geometry of the $D \to \infty$ limit. This approach has elucidated pseudo-molecular aspects of intrashell excited states of two-electron atoms [86,97–99,107] and shown how to exploit exact and approximate interdimensional degeneracies [107,108]. Highly accurate calculations for several excited two-electron atomic states have also been made by developing $1/D$ perturbation series to high order [109,110].

Here we present an unconventional method [111] that provides useful accuracy for some states yet requires only simple zero-order calculations and can be readily applied to excited states of multielectron atoms. It involves incorporating the principal and orbital angular momentum quantum numbers in the D-scaling parameters.

6.1. *Introducing n and L as scaling parameters*

The strategy is to modify the Laplacian and Jacobian for He S-states, as given in Table 1. As proposed in [111], the $D-1$ and $D-2$ indices are replaced with generalized parameters:

$$\gamma_1 = n_1(D-1), \tag{6.1a}$$

$$\gamma_2 = n_2(D-1), \tag{6.1b}$$

$$\alpha = L(D-2), \tag{6.1c}$$

where n_i and L are finite positive integers; thus γ_i and α will tend to infinity along with D. Introducing the parameters n_i and L provides additional degrees of freedom in the final energy expression. This parametrization can be interpreted as the cardinality of a space, larger than D dimensions, which includes the energy levels of the physical system.

Then

$$\nabla_1^2 + \nabla_2^2 = K_{\gamma_1}(r_1) + K_{\gamma_2}(r_2) + \left(\frac{1}{r_1^2} + \frac{1}{r_2^2}\right) L_\alpha^2, \tag{6.2}$$

where

$$K_\gamma(r) = \frac{1}{r^\gamma}\frac{\partial}{\partial r} r^\gamma \frac{\partial}{\partial r} \tag{6.3a}$$

$$L_\alpha^2 = \frac{1}{\sin^\alpha\theta}\frac{\partial}{\partial\theta}\sin^\alpha\theta\frac{\partial}{\partial\theta}. \tag{6.3b}$$

The corresponding Jacobian is $J_{\gamma-\alpha} = r_1^{\gamma_1} r_2^{\gamma_2} \sin^\alpha\theta$. When the new Laplacian of Equation (6.2) acts on a wavefunction of the form $\Psi_D = J^{-1/2}\Phi_D$, we obtain via the

usual hydrogenic scaling in the $D \to \infty$ limit a simple energy expression

$$E(n_1, n_2, L) = \frac{1}{2}\left(\frac{n_1^2}{r_1^2} + \frac{n_2^2}{r_2^2}\right) + \frac{L^2}{2}\left(\frac{1}{r_1^2} + \frac{1}{r_2^2}\right)\cot^2\theta + V(r_1, r_2, \theta). \tag{6.4}$$

This offers a simple means to obtain atomic excited states by associating n_i as the principal quantum number for electron i and assigning L in an appropriate fashion. A nominal assignment was proposed [111], $L = \ell_1 + \ell_2$, simply the sum of the individual hydrogenic orbital angular momentum quantum numbers. That is the maximum among the set of values arising from vector addition: $[|\ell_1 - \ell_2|, |\ell_1 - \ell_2 + 1|, \ldots, |\ell_1 + \ell_2|]$.

Energies obtained in this way by minimizing Equation (6.4) were presented in [111] for several S, P, and D excited states of He. An analogous treatment for some excited states of Li and Be was also given. Agreement with conventional $D = 3$ electronic structure results was good, typically better than 1%, even without recourse to adding any $1/D$ perturbation terms.

However, such use of Equation (6.4) and kindred results requires a serious amendment, only recognized in preparing this review. First, note that the energy, $E = E_S + E_L$, separates into terms present for S-states ($L = 0$),

$$E_S(n_1, n_2) = \frac{1}{2}\left(\frac{n_1^2}{r_1^2} + \frac{n_2^2}{r_2^2}\right) + V(r_1, r_2, \theta), \tag{6.5′}$$

plus terms that enter for non-S states ($L > 0$),

$$E_L(L) = \frac{L^2}{2}\left(\frac{1}{r_1^2} + \frac{1}{r_2^2}\right)\cot^2\theta. \tag{6.6′}$$

Equation (6.5′) indeed corresponds to the form obtained for a Bohr model using his momentum quantization rule ($p = n/r$), as noted in Equation (2.12). But this is not consistent with use of the full Jacobian in deriving Equation (6.4); for the ground S-state that requires the centrifugal term to contain a factor of $1/\sin^2\theta$, as seen in Table 1. The source of this inconsistency is readily traced to the definition of α adopted in Equation (6.1). In order to obtain the correct Hamiltonian for the ground S-state (with $n_1 = n_2 = 1, L = 0$), we must have $\alpha = D - 2$ rather than $\alpha = 0$. To accommodate this constraint, we instead define $\alpha = \alpha_0(D - 2)$, where $\alpha_0 = 1 + \alpha_L$ and all dependence on angular momentum quantum number(s) appears in α_L, yet to be specified. In Equation (6.4) this merely replaces L^2 with $(1 + \alpha_L)^2$ but the E_S and E_L terms become

$$E_S(n_1, n_2) = \frac{1}{2}\left(\frac{n_1^2}{r_1^2} + \frac{n_2^2}{r_2^2}\right) + \frac{1}{2}\left(\frac{1}{r_1^2} + \frac{1}{r_2^2}\right)\cot^2\theta + V(r_1, r_2, \theta,) \tag{6.5}$$

and

$$E_L(L) = \frac{\alpha_L(\alpha_L + 2)}{2}\left(\frac{1}{r_1^2} + \frac{1}{r_2^2}\right)\cot^2\theta. \tag{6.6}$$

As discussed below, in Section 6.2, our amended definition of α is essential to model the most probable interelectron angle, θ_m for S-states and thereby enable realistic assessment of electron–electron correlation.

At present, treatment of non-S states by Equation (6.4) remains in limbo because a satisfactory way to specify α_L has not been found. The comparisons with $D=3$ results in [111] proved misleading. For most of the non-S states considered, θ_m is not far from 90°; thus, in Equations (6.4) and (6.6) the factor $\cot^2\theta$ is so close to zero that $E_S \gg E_L$. Accordingly, the value adopted for α_L has little effect for such states. Also, the choice ($\alpha_0 = L$) originally made for α in Equation (6.1) led in [111] to misassigning S states as P states. A useful choice for α_L would require specifying more quantum numbers than the total angular momentum alone. Further efforts to extend quantum number D-scaling to non-S states may find guidance from an extensive analysis by Dunn and Watson of the large-D limit of higher angular momentum states of two electron atoms [108] as well as insightful models that restrict the electrons to the surface of a sphere [112].

6.2. *Generic geometric aspects of excited electronic states*

As emphasized in Section 5.3, minimizing the energy expression for the Bohr model for He gives $\theta = 180°$ for all S-states. However, as illustrated in Figure 26 and Table 3, for the ground S-state the most probable interelectron angle, θ_m, occurs only a few degrees above 90°. In Figure 27 we contrast the variation of θ_m for two species of excited states: (a) Rydberg states, with $n_1 \ll n_2$, for which θ_m declines towards 90° with increasing excitation, and (b) intrashell states, with $n_1 = n_2$, for which θ_m climbs towards 180°. In Figure 28 we show the corresponding energies and most probable radii. For the Rydberg states (Figure 28a), when n_2 substantially exceeds n_1, the corresponding electron radii become very different (since $r \sim n^2$), so their angular correlation fades away and $\theta_m \to 90°$, the uncorrelated value. The outer electron then sees a screened nucleus with charge near $Z \sim 1$, so as n_2 grows the energy rapidly approaches

$$E \to -\frac{1}{2}\left[\frac{Z^2}{n_1^2} + \frac{(Z-1)^2}{n_2^2}\right], \tag{6.7}$$

a double hydrogenic limit for which D-scaling by design becomes exact. For intrashell states (Figure 28b), with increasing excitation, both electrons retreat further from the nucleus and as their radii are on average equal, their angular correlation becomes increasingly pronounced and $\theta_m \to 180°$, the maximally correlated value. In intrashell states the electronic distribution thus exhibits marked pseudo-molecular character with only vestigial hydrogenic traces.

7. Other Bohr-style applications

The topics we now consider involve electronic structure subject to potentials that differ markedly from purely Coulombic interactions. These include the interaction of atoms with extremely strong magnetic fields or with superintense laser fields. Our chief aim is to illustrate further aspects of the large-D limit as a semiclassical approximation method.

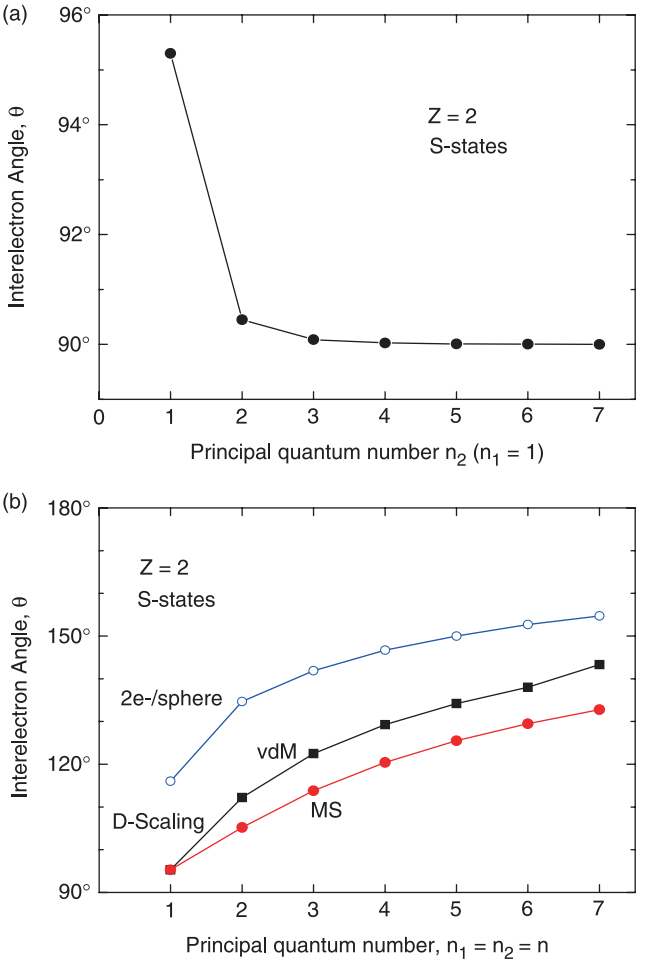

Figure 27. θ_m for two species of excited states: (a) Rydberg ($1s^1ns^1\,S$) states. Dots obtained from Equation (6.5); (b) intrashell ($ns^2\,S$) states. 'MS' (dots) are calculated from Equation (6.5), 'vdM' (squares) from van der Merwe [97–99], and $2e^-/sphere$ (circles) from model calculations for two-electrons on a rigid sphere (taken from Herschbach *et al.* [86]).

7.1. *H atom in superstrong magnetic fields*

The energy level structure induced by strong magnetic fields has a prominent role in many problems in astrophysics and solid-state physics, as well as in atomic physics [114]. For the H atom, a wide variety of approximation methods have been studied, because the Hamiltonian is non-separable and there is no natural perturbation parameter valid at both high and low fields. Exact calculations are now feasible for any field strength, by means of modern computing power. However, in addition to heuristic value, semiclassical approximations [115,116] remain useful, e.g., for calculating quantities such as partition functions that require evaluation of myriad energy levels.

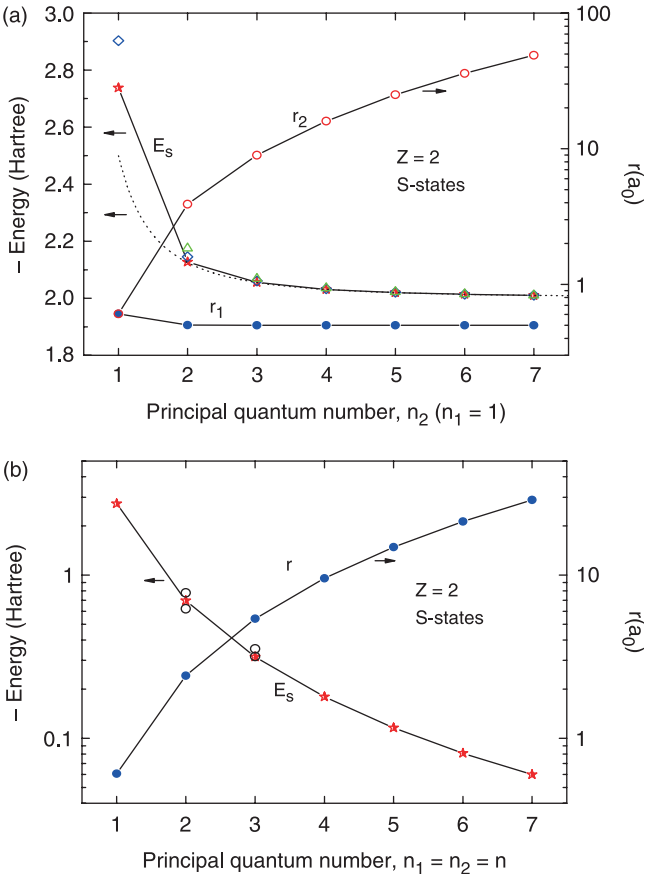

Figure 28. Energy and most probable radii for two species of excited states: (a) Rydberg ($1s^1ns^1\,S$) states. Stars are optimized energies from Equation (6.5); dotted curve is the energy curve from Equation (6.7); diamonds and triangles are experimental energies for ^1S and ^3S states respectively [53]; circles and dots are the most probable radii for the outer and inner electrons. (b) intrashell ($ns^2\,S$) states. Stars are energies from minimizing Equation (6.5); circles are corresponding energies taken from Lindroth [113]; dots are the most probable radii, $r_{1m} = r_{2m}$, of the electrons.

For a hydrogen atom in a uniform magnetic field B along the z axis, the energy levels are $E + \frac{1}{2}mB$, where m is the magnetic quantum number and E an eigenvalue of $H = T + U + V$, with

$$T = -\frac{1}{2}\left(\frac{\partial^2}{\partial\rho^2} + \frac{\partial^2}{\partial z^2}\right),$$
$$U = \frac{1}{2}\frac{\Lambda(\Lambda+1)}{\rho^2}, \tag{7.1}$$
$$V = -\left(\rho^2 + z^2\right)^{-1/2} + \frac{1}{8}B^2\rho^2.$$

In atomic units, $B=1$ corresponds to a field strength of $m_e^2 ce^3/\hbar^3$, which is approximately 2.35×10^5 tesla. The dependence on D and $|m|$ enter only in the quantity $\Lambda = |m| + \frac{1}{2}(D-4)$. Interdimensional degeneracies therefore occur between states with angular momentum along the z-axis of $|m|$ in D dimensions and states with $|m|-\mu$ in $D+2\mu$ dimensions [117,118]. Since changing D is equivalent to changing $|m|$, we will retain $D=3$ and instead use $|m|\to\infty$ to carry out scaling. We define $\delta = 1/(|m|+a)$, where the shift constant a is included to preserve δ as a finite parameter at $m=0$. Then we scale units via

$$\rho = \delta^{-2}\tilde{\rho}, \quad z = \delta^{-2}\tilde{z},$$

$$E = \delta^2 \tilde{E}, \quad B = \delta^3 \tilde{B}, \tag{7.2}$$

which transform the Hamiltonian via

$$T \to \delta^2 \tilde{T}, \quad U \to \left(1 - 2a\delta + \left(a^2 - \frac{1}{4}\right)\delta^2\right)\tilde{U}, \quad V \to \tilde{V}, \tag{7.3}$$

where $\tilde{T} = T(\tilde{\rho}, \tilde{z})$, etc. For large $|m|$, the factor of δ^2 plays the role of $\hbar^2$ in the Schrödinger equation for a particle of unit mass subject to an effective potential $\tilde{W} = \tilde{U} + \tilde{V}$. In the limit $\delta \to 0$, all the eigenvalues collapse to

$$\tilde{E}_0 = \tilde{W}(\tilde{\rho}_m, \tilde{z}_m), \tag{7.4}$$

at the minimum of the effective potential. There $\tilde{z}_m = 0$ and $\tilde{\rho}_m$ is found as a positive root of the equation $\tilde{B}^2\tilde{\rho}_m^4 = 4(1-\tilde{\rho}_m)$. Thus, as $|m|\to\infty$, the electron becomes localized on a circular orbit of radius $\tilde{\rho}_m$, which shrinks to zero in the strong field limit, $B\to\infty$. A formulation suitable for the entire range of field strengths is obtained via a further scaling [118],

$$\xi = \tilde{\rho}/\tilde{\rho}_m, \quad \eta = \tilde{z}/\tilde{\rho}_m, \quad \varepsilon = \tilde{\rho}_m^2 \tilde{E}_0. \tag{7.5}$$

This recasts the effective potential as

$$W(\xi,\eta) = \frac{1}{2\xi^2} - \frac{1-g}{(\xi^2+\eta^2)^{1/2}} + \frac{1}{2}g\xi^2, \tag{7.6}$$

where $g = 1-\tilde{\rho}_m = \tilde{B}^2\tilde{\rho}_m^4/4$. Variation of g from zero to unity corresponds to varying the field strength from zero to infinity,

$$\tilde{B} = 2g^{1/2}(1-g)^{-2}. \tag{7.7}$$

At the $|m|\to\infty$ limit, the classical dynamics of the rescaled circular orbit do not depend on the magnetic field, since ξ_m and the orbital velocity $1/\xi_m$ remain unity. Fluctuations about this orbit for $|m|<\infty$ may be incorporated by introducing δ-scaled displacement coordinates, defined by $\xi - 1 = \delta^{1/2}q_1$, $\eta = \delta^{1/2}q_2$, and expanding $W(\xi,\eta)$ as

$$W = W_m(1,0) + \delta\left(\frac{1}{2}\omega_1^2 q_1^2 + \frac{1}{2}\omega_2^2 q_2^2 - a + \cdots\right). \tag{7.8}$$

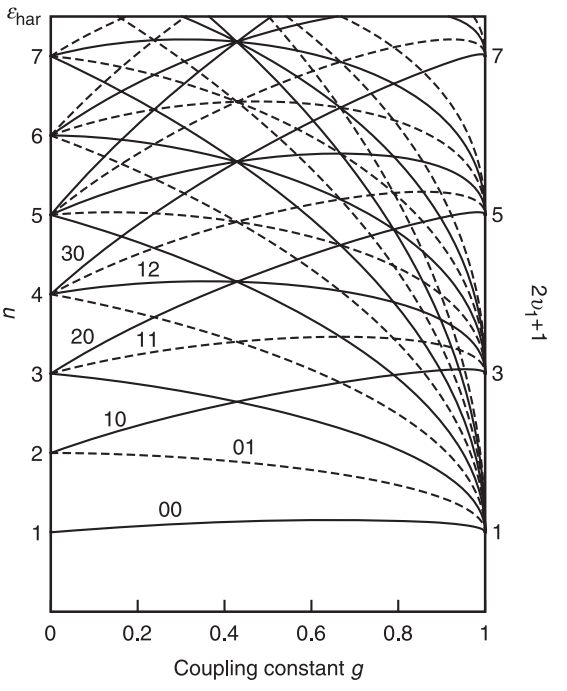

Figure 29. The rescaled vibrational energy of the even parity states (solid curves) and odd parity states (dashed curves) in the large m limit. The curves are labelled by harmonic oscillator quantum numbers v_1, v_2. From [119].

Here $W_m(1,0) = \tilde{\rho}_m^2 \tilde{E}_0 = -\frac{1}{2} + \frac{3}{2}g$ and the terms linear in δ correspond to a pair of independent harmonic oscillators, q_1 and q_2, vibrating perpendicular and parallel to the magnetic field, respectively, with frequencies $\omega_1 = (1+3g)^{1/2}$ and $\omega_2 = (1-g)^{1/2}$.

Figure 29 plots the contribution of these harmonic vibrations to the scaled energy levels, $\varepsilon = \varepsilon_0 + \delta(\varepsilon_{har} - a) + \cdots$, given by

$$\varepsilon_{har}(g) = \omega_1\left(v_1 + \frac{1}{2}\right) + \omega_2\left(v_2 + \frac{1}{2}\right). \tag{7.9}$$

At the zero field limit, the H atom is unperturbed; $\omega_1 = \omega_2 = 1$ and the vibrational terms, $\varepsilon_{har}(0) = v_1 + v_2 + 1$, group into bunches associated with different values of the principal Coulombic quantum number, with $n = v_1 + v_2 + 1$. Since in the zero field limit

$$E = \delta^2 W_m(1,0) = -\frac{1}{2}(|m| + a)^{-2}, \tag{7.10}$$

the shift parameter is specified as $a = v_1 + v_2 + 1$, to conform at $|m| = 0$ to the exact hydrogenic energy levels. In the high field limit, $\omega_1 = 2$, $\omega_2 = 0$, $\varepsilon_{har}(1) = 2v_1 + 1$, and the terms cluster into Landau resonances. When $g = 3/7$, the ratio of frequencies is 2 : 1, and a host of curve-crossings occur, akin to Fermi resonances in molecular vibrations. Many other such crossings occur, stemming from branch point singularities which can be identified in the complete δ plane [117]. Anharmonic contributions from terms higher

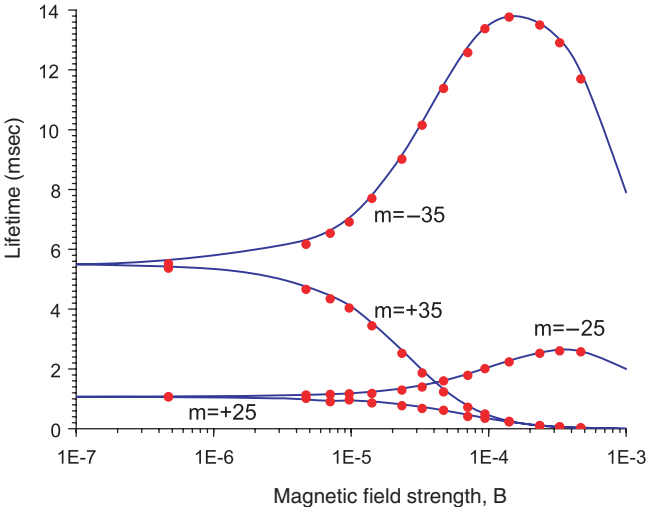

Figure 30. Radiative lifetimes of the $m = \pm 25$ and ± 35 circular Rydberg states of H as a function of the magnetic field strength B (in units of 2.35×10^5 tesla). Full curves computed from harmonic oscillator approximation [120], points from high-order perturbation expansion [121]. Figure taken from Ref. [120].

order in δ convert the crossings into avoided intersections ('anti-crossings') and otherwise shift levels increasingly as $|m|$ decreases.

Of special interest are circular Rydberg states with $|m| = n - 1$. In the field-free atom these have exceptionally long radiative lifetimes and resemble the Bohr model increasingly for large $|m| \gg 1$. Even for high fields, for such states it is often adequate to include just the harmonic oscillations about the orbit [120,121]. Figure 30 illustrates the impressive accuracy obtained by simply using first-order harmonic oscillator wavefunctions to calculate the lifetimes of some circular states, over a range of magnetic field strength extending to about 10^2 tesla, which is above laboratory limits.

7.2. *Atom ionization inhibited by superintense laser fields*

High-frequency superintense laser fields induce exotic and often paradoxical electronic properties of atoms [122]. A particularly striking aspect is that the ionization probability decreases as laser intensity increases [123]. Moreover, it becomes possible to bind 'extra electrons'. Calculations employing Floquet theory have predicted stabilization of multiply-charged anions of hydrogen [124] and doubly charged anions of helium and lithium atoms [125]. As yet, such stabilization has not been demonstrated experimentally, except for atoms initially prepared in a Rydberg state [126].

The predicted stabilization of atomic anions is accompanied by splitting of the electronic charge distribution into lobes governed by the polarization of the laser field. This localization of the electrons markedly reduces encounters with the nucleus as well as electron correlation and hence suppresses autoionization [123,127]. Such pronounced localization suggests that the pseudoclassical large-D limit might provide a useful approximation. Indeed, a Bohr-style model has proved to work well for evaluating the

detachment energy as a function of the laser field parameters [128]. As the large-D limit requires far simpler computations than $D=3$, it can facilitate examining prospects for other effects induced by superintense laser fields.

We consider a high-frequency monochromatic electric field with amplitude E_0 and frequency ω incident on an N-electron atom. In the dipole approximation, each electron is subjected to the same field and undergoes quiver oscillations $\alpha(t)$ along a trajectory given by

$$\alpha(t) = \alpha_0(\mathbf{e}_1 \cos\omega t + \mathbf{e}_2 \tan\delta \sin\omega t), \tag{7.11}$$

where the quiver amplitude is $\alpha_0 = E_0/\omega^2$. The spatial orientation of the oscillations is specified by $\mathbf{e}_1$ and $\mathbf{e}_2$, unit vectors orthogonal to each other and to the propagation direction of the laser; $\delta = 0$ corresponds to linear polarization and $\delta = \pm\pi/4$ to circular polarization. In a reference frame (KH, for Kramers–Henneberger), translated by $\alpha(t)$ with respect to the laboratory frame, the electrons no longer quiver, while instead the nucleus quivers along the $\alpha(t)$ trajectory. In the KH frame, the Coulombic attraction between any electron and the nucleus takes the form $-Z/|\mathbf{r}_i + \alpha(t)|$, where Z is the nuclear charge. Thus, in the KH frame, the atomic structure corresponds essentially to the large-D limit, except that the nuclear charge is no longer located in a point but rather is smeared out, in a fashion governed by the quiver amplitude, frequency dependence, and polarization of the laser field.

The high-frequency Floquet theory (HFFT) pertains when the field frequency is high compared with the excitation energy of the atom in the field. Then the electrons feel a time-averaged effective potential, termed the 'dressed potential', given by

$$V_0(\mathbf{r}_i, \alpha_0) = -\frac{Z}{2\pi}\int_0^{2\pi\omega} \frac{\mathrm{d}\Omega}{|\mathbf{r}_i + \alpha(t)|}, \tag{7.12}$$

where $\Omega = \omega t$ and the average extends over one period of the laser field. The corresponding Schrödinger equation in the KH frame is

$$\sum_{i=1}^{N}\left[\frac{1}{2}\mathbf{p}_i^2 + V_0(\mathbf{r}_i, \alpha_0) + \sum_{j=1}^{i-1}\frac{1}{|\mathbf{r}_i - \mathbf{r}_j|}\right]\Phi = \varepsilon(\alpha_0)\Phi. \tag{7.13}$$

The field parameters E_0 and ω appear only in the dressed potential and enter only via α_0, the quiver amplitude. Of prime interest is the detachment energy required to remove one of the N electrons,

$$DE^{(N)}(\alpha_0) = \varepsilon^{(N-1)}(\alpha_0) - \varepsilon^{(N)}(\alpha_0), \tag{7.14}$$

determined by the energy eigenvalues obtained from Equation (7.13). As long as $DE > 0$, the N-electron atom or ion remains stable with respect to loss of an electron and thus supports at least one bound state. This stabilization requires $\alpha_0 > \alpha_0^{\mathrm{crit}}$, the critical quiver amplitude for which $DE = 0$. At some higher value, denoted by $\alpha_0^{\max}$, the DE reaches its maximum positive value and as α_0 increases further DE eventually returns to zero.

Figure 31 shows $DE(\alpha_0)$ functions obtained from the large-D version of HFFT, as applied to hydrogen or helium atoms with $N = 2, 3, 4$ in superintense laser fields with linear polarization [128]. The agreement with results from conventional $D=3$ calculations is very good.

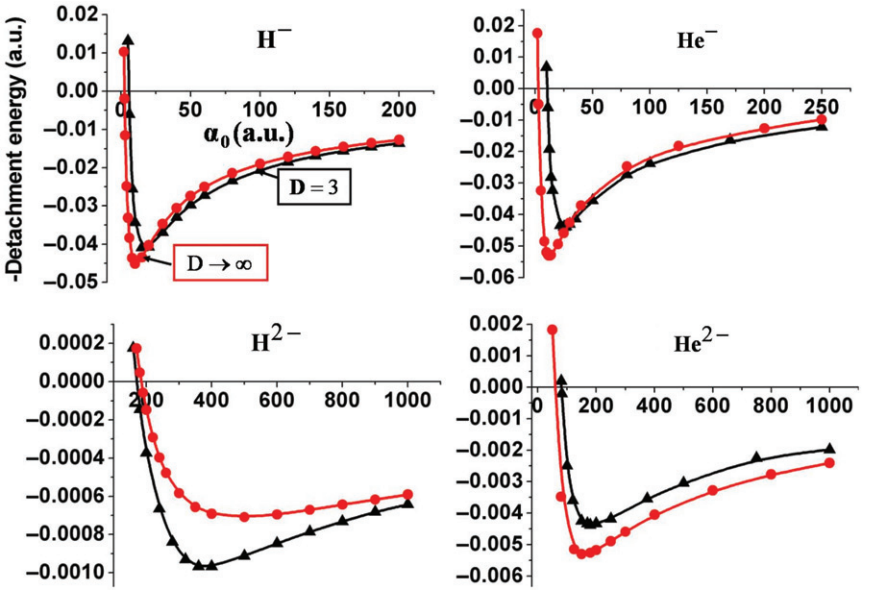

Figure 31. Negative of detachment energy, $-DE^{(N)}(\alpha_0)$, for removal of an electron as a function of the quiver amplitude, α_0, for the ground states of H^-, H^{2-}, He^-, and He^{2-} in the high frequency limit of linearly polarized laser fields. Results, from [128], are shown for $D=3$ and the large-D limit.

In the D-scaling treatment, it is convenient to use cylindrical coordinates, in view of the axial symmetry that obtains for either linear or circular polarization. Because for large α_0 there is virtually no overlap among lobes of the electron distribution, electron correlation can be neglected, so only the Hartree–Fock (HF) case need be considered. At the large-D limit the effective Hamiltonian corresponding to Equation (7.13) then becomes

$$W=\frac{1}{2}\sum_{i=1}^{N}\frac{1}{\rho_i^2}+\sum_{i=1}^{N}V_0(\rho_i,z_i,\alpha_0)+\sum_{i=1}^{N}\sum_{j=i+1}^{N}\frac{1}{\sqrt{\rho_i^2+\rho_j^2+(z_i-z_j)^2}}, \tag{7.15}$$

where for the ith electron, ρ_i measures the distance from the polarization axis, z_i is the distance along that axis. For linear polarization, the dressed electron–nucleus interaction is given by

$$V_0(\rho_i,z_i;\alpha_0)=-\frac{Z}{2\pi}\int_0^{2\pi}\frac{\mathrm{d}\phi}{\sqrt{\rho_i^2+(z_i-\alpha_0\sin\phi)^2}}. \tag{7.16}$$

All distance coordinates, including α_0, are scaled by κ^2 and energies by κ^{-2}, with $\kappa=(D-1)/2$. Except for the dressed potential, Equation (7.15) corresponds simply to a Bohr-style model; the first term is the centrifugal contribution from the kinetic energy, the third is the electron–electron repulsion, simplified in form because the dihedral angle between any pair of electrons, $\phi_i-\phi_j=90^\circ$ in the HF large-D limit [96]. By minimizing Equation (7.15) we obtain the energy $\varepsilon^{(N)}$ as well as the positions of the localized electrons as functions of α_0. As verified in the $D=3$ calculations, because the relevant range of α_0 is

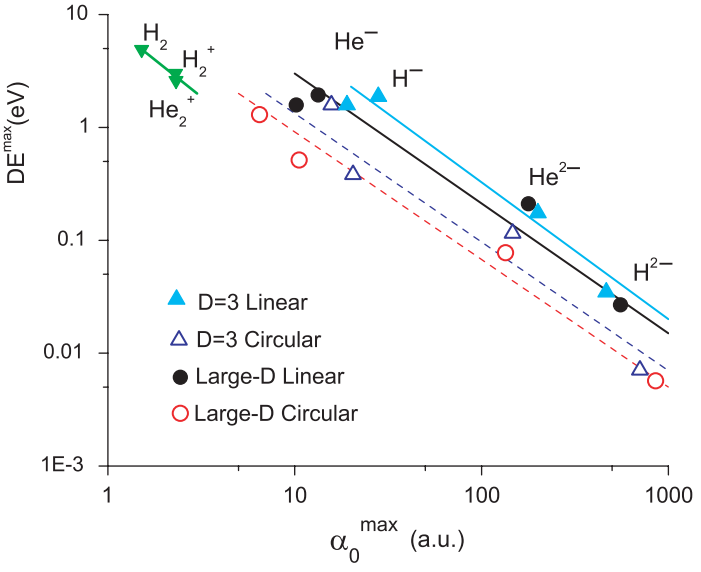

Figure 32. Log-log plot of the detachment energy (eV) as a function of $\alpha_0^{\max}$ (a.u.) for the ground state of H^-, H^{2-}, He^-, and He^{2-} at $D=3$ and $D=\infty$ in linearly and circularly polarized superintense laser fields. For analogy we plot on the top left side corner a Log-Log plot of the dissociation energy as a function of the internuclear distance at $D=3$ for the molecules H_2, H_2^+ and He_2^+. Note the similarity in behaviour of atoms in superintense laser fields and their equivalent diatomic molecules.

so large, the overlap of one-electron orbitals is negligibly small [128]. Accordingly, the HF exchange terms are likewise negligible and since the Hamiltonian is independent of spin, the eigenvalues are degenerate with respect to spin. For circular polarization, the procedure is the same except reorienting the quiver amplitude, which changes the form of the dressed potential.

As seen in Figure 31, the dependence of the electron detachment energy on quiver amplitude resembles the potential energy curve for stretching a chemical bond, although $DE^{\max}$ is much smaller than typical bond dissociation energies and $\alpha_0^{\max}$ is very much larger than equilibrium bond lengths. Figure 32 shows that the correlation between $DE^{\max}$ and $\alpha_0^{\max}$ is actually similar to, but not as steep, as that between bond strengths and lengths for H_2, H_2^+, and He_2^+ molecules. This correlation extends over three orders of magnitude and is much the same for linear and circular polarization and whether $D=3$ or the large-D limit.

These results, obtained from a rudimentary version of D-scaling, encourage applications to exploratory studies of other superintense laser processes, particularly involving electron localization. Inviting opportunities include evaluating the large-D limit of HFFT for molecules and incorporating time dependence to examine ionization lifetimes and dynamics at laser intensities below the threshold for stabilization.

8. Conclusions and outlook

In this review, our chief aim has been to illustrate how well the newly resurrected Bohr model and kindred large-D approximations can simulate major features of few-electron

atoms and molecules. The ease and simplicity with which these methods provide modest but useful accuracy and heuristic insights are their main virtues. Accordingly, we have limited consideration almost entirely to the large-D limit. We conclude with comments about broader aspects of this limit, first noting its curious relation to rival prequantum models of atomic structure and chemical bonding. We point out also how in the large-D limit the changes in electronic geometry that occur as bonds are stretched correspond to introducing alternative resonance structures in wave mechanics. We then consider prospects for joining D-scaling with other methods to extend its utility and scope.

8.1. *New perspectives on old models*

The large-D limit belatedly reconciles the Bohr model with the more rudimentary prequantum 'static atom' model advanced in 1916–23 by Gilbert Newton Lewis and by Irving Langmuir. An excellent historical account is given in a forthcoming book by Patrick Coffey [129]. Like the Bohr model, the Lewis–Langmuir model still has a semantic role, even beyond introductory texts. Relying on his intuition and wide empirical perspective, Lewis proposed that chemical bonds generally were formed by shared electron pairs [40]. This key idea enabled him to interpret a host of chemical observations, although he visualized atoms as cubical, with electrons perched at the corners. He objected to Bohr's picture of orbiting electrons, as Lewis felt it could not explain the stability and geometry of molecules and crystals. Langmuir became an ardent advocate of largely static models, but eventually suggested atoms were likely spherical and that 'the electrons could ... rotate, revolve, or oscillate about definite positions in the atom' [48]. Most chemists in that era were content to draw 'Lewis dot' diagrams of molecules, blithely guessing where to locate the valence electrons forming bonds. Physicists viewed such static models with distain; Robert Millikan in 1924 assailed the Lewis model as 'electrons sitting around on dry goods boxes at every corner, ready to shake hands with, or hold onto similar loafer electrons in other atoms' [130].

In the $D \to \infty$ limit, however, the electrons do become loafers. In the D-scaled space, they assume fixed positions relative to the nuclei and each other that correspond to the minimum of the effective potential, $U + V$. In homage, this has been termed the *Lewis structure* [24]. It can be calculated exactly from classical electrostatics and thus provides a rigorous version of the qualitative electron-dot formulas introduced by Lewis in 1916. Indeed, Loeser obtained a fair approximation (Figure 6), in his treatment of many-electron atoms at large-D [68], after reducing the problem to only one radial and one angular variable by assuming that the electrons reside at the corners of a regular simplex, a 'hypertetrahedron' version of Lewis' cubical atom. In the recent analysis by Sergeev of the Bohr model for large atoms [66], minimizing our Equation (2.12), he found that as N increases the electrons within each shell do in fact assume a symmetrical simplex geometry.

For D finite but very large, the electrons are confined to harmonic oscillations about the fixed positions attained in the $D \to \infty$ limit; this corresponds to the first-order perturbation term, proportional to $1/D$, and is calculable from the curvatures of the effective potential about its minimum. The $1/D$ contributions, which prod the loafer electrons into shuffling and swaying, have been termed *Langmuir vibrations* [24], to acknowledge the prescient suggestion he made in 1919. In the large-D limit, the Bohr, Lewis and Langmuir models merge.

The large-D limit also offers a new perspective on another aspect of chemical bonding that, in its historical context, had provoked controversy [26]. This is the concept of *resonance* between alternative valence-bond structures, advocated with evangelical zeal by Linus Pauling [54]. Many polemical attacks repeatedly pointed out that the exchange or resonance integrals, exemplified in the prototype Heitler–London treatment of H_2, do not appear in less approximate treatments. By extension, the critics concluded that for any molecule resonance is an artifact, a misleading consequence of using a particular variational form to approximate the wavefunction.

In the large-D limit, as illustrated for H_2 in Sections 2.1 and 3.1 (cf. Figures 3 and 8), the effective potential $U+V$ and hence the electron distribution changes form as the internuclear distance varies. Thus, $U+V$ exhibits minima that correspond to a different Lewis structure for each distinct valence bond configuration. At small R, there is a single minimum and the electrons reside in the plane bisecting the internuclear axis (H:H dot structure). At larger R, two pairs of double minima emerge [14,35]. One pair corresponds to localizing each electron on a different nucleus ($\mathrm{H}\cdot + \mathrm{H}\cdot$); the other pair, much less favourable energetically, has both electrons on one or the other nucleus (H:+H and H+H:). Tunnelling of the electrons among these various minima in the effective potential corresponds to resonance among the different Lewis structures. In valence-bond theory, these structures are represented by different approximate wavefunctions. However, it is satisfying that the large-D limit, which does not involve assumptions about the wavefunction, clearly exhibits the equivalent of Pauling resonance among distinct Lewis structures.

8.2. *Prospects for wider use of D-scaling*

The fixed electronic geometry attained in the large-D limit, a pointwise delta-function, differs drastically from a $D=3$ wavefunction and moreover lacks exchange and shell structure. It thus is surprising that such an unrealistic model nonetheless offers useful information for determining $D=3$ results, particularly about electron correlation. An instructive analysis has been given by Loeser and colleagues [131]. A crucial feature is that the pointwise large-D structure exists in the scaled space, not the 'real world'. All electronic positions have components outside the $D=3$ physical subspace, and those hyperdimensional components significantly enhance the ability of a localized structure to represent the true solution and to model it quantitatively. As noted in Section 2.2, in treating the Bohr model for large atoms, Sergeev exploited a kindred aspect and got substantially improved accuracy.

Also surprising, as seen in Sections 2 and 3, is that fairly good molecular potential curves for diatomic chemical bonds can actually be obtained simply by minimizing an algebraic function, $U+V$, derived from the large-D limit and equivalent to classical mechanics. Determining the energy from $U+V$ indeed amounts to generalizing the balance of centrifugal and Coulombic interactions invoked by Bohr in his 1913 treatment of the H atom. It can also be regarded as generalizing the estimate of the H atom size and energy obtained from a pedagogically appealing uncertainty principle argument. As presented by Feynman [132]: if the spread in position of the electron is of order a, the spread in its momentum is of order h/a, thus the sum of the kinetic energy and potential energy is roughly $E \approx h^2/2ma^2 - e^2/a$; minimizing this gives $a = h^2/me^2$, the Bohr radius,

and $E = -e^2/2a$, the Rydberg. (Since a is only vaguely defined, the results are contrived but 'the idea is right'.) In effect, the D-scaling procedure serves to incorporate the uncertainty principle, while morphing the Schrödinger equation into Newtonian mechanics at the large-D limit.

As noted in Section 2, despite its localization of the electrons, the large-D limit is fully consistent with the uncertainty principle. Because the coordinate localization occurs in the D-scaled space, the conjugate momenta are scaled inversely, so the position-momentum commutator remains invariant in that space, for any D-value. This key aspect of quantum mechanics is discreetly hidden in the choice of D-dependent distance units. Hence, seemingly classical calculations at large-D are still quantum mechanical. In particular, electronic tunnelling can be computed as if the electrons sat motionless at the minima of a classical electrostatic potential in D-scaled space, because the scaling relates this limit to the quantum fluctuations that actually occur in the physical $D = 3$ subspace [133,134] (for commentary, see also [14] and [26]). Thereby a property, regarded as quintessentially quantal, can be approximated fairly well by a purely classical calculation.

Another virtue of D-scaling is that it treats the full Hamiltonian. Thus, in principle, the ability to approximate $D = 3$ results does not depend directly on the magnitude of interactions, or the extent of non-separability or correlations among variables, but rather depends chiefly on the D-dependence. A straightforward way to go beyond the $D \to \infty$ limit is a perturbation expansion in $1/D$, or in a related quantity such as $1/(D - s)$, with s a shift parameter chosen by some auxiliary criterion (as in Section 7.1). We merely note here some references that evaluate the first-order $1/D$ contribution, the harmonic Langmuir vibrations [14,18,68,111]. For atoms this is relatively easy and usually improves quantitative results appreciably. For atoms, efficient algorithms for computing and summing large-order anharmonic $1/D$ terms have been developed [19,20,112,135]. These appear capable of providing highly accurate solutions of the exact Schrödinger equation for atoms with as many as 10 coupled internal degrees of freedom. Also, Goodson has formulated a self-consistent-field theory which invokes separability in terms of large-D normal vibrational coordinates, each of which describe correlated motion of many particles [135]. This offers a practical means to treat much larger atoms.

For molecules, however, the $1/D$ perturbation expansion is much less tractable. Even evaluating the first-order term is troublesome, because it involves the curvature of the large-D effective potential, $U + V$, which often changes abruptly as R (or other geometrical parameters) are varied and the Lewis structure changes. In deriving the $E(R)$ potential energy curve for H_2, as in Figures 2 and 9, we computed the $1/D$ term but found it introduced an unpalatable sharp cusp near the equilibrium bond distance. This resulted from the symmetry breaking illustrated in Figure 3, which switches the electron distribution from unimodal to bimodal. The same effect is prominent for H_2^+; an insightful analysis by Tan and Loeser brought out reasons why the critical R for the symmetry breaking occurs near the equilibrium bond distance [101,102]. Such switches among distinct Lewis structures have the character of phase transitions [136–139] and will be ubiquitous for molecules. Hence other methods not involving even the first-order $1/D$ term are more inviting for molecules, such as the interpolation and constraint techniques illustrated in Sections 3 and 4.

For further development of Bohr-like models and D-scaling treatments of electronic structure, it appears most practical to focus chiefly on the large-D limit. Some applications,

such as presented in Section 7, do not require high accuracy but involve unusually awkward or tedious computations if treated by conventional quantum mechanics. There are also opportunities to enhance the scope and efficacy of the D-scaling used to obtain the large-D limit. The contrast in Section 5 between the Bohr model for H_2 and its united atom, He, suggests that results for molecules might be improved by introducing R-dependence in the D-scaling. For instance, that could be done by adjusting the Jacobian, in the fashion of Section 6, so that the appropriate angular factors appear in the united atom limit but are quenched elsewhere for the sake of enhancing chemical bonding.

A general procedure for modifying the $D \to \infty$ limit has been developed by Loeser to render it more realistic in modelling $D = 3$ electronic structure [140]. This involves constructing subhamiltonians, qualitatively similar to the Bohr-like pseudoclassical $U + V$ forms we have considered. These are augmented by 'prescalings' that build in both shell structure and generic aspects of radial and angular nodal structure, guided by hydrogenic or SCF results. Although thus far applied mostly to atoms, Loeser emphasizes that subhamiltonians for molecules and solids can be constructed in essentially the same way. He regards the 'primary appeal of the method is its ability to model correlation effects . . . [with] no use of basis sets'.

Another approach, likewise motivated by the simplicity of the large-D limit, is to seek ways to meld it directly with $D = 3$ methods [28]. This strategy has thus far been used in two versions that combine large-D with Hartree–Fock (HF) results. As applied to many-electron atoms, both involve using the large-D limit to find a renormalized nuclear charge that yields an improved approximation to the $D = 3$ energy. In the version (denoted A) tried first, the renormalized charge, $Z + \Delta Z$, was determined via

$$E_\infty^{\mathrm{HF}}(N, Z + \Delta Z) \equiv E_3^{\mathrm{HF}}(N, Z). \tag{VIII.1a}$$

The corresponding $D = 3$ approximation [141–143] (for commentary, see also [14] and [27]) is then obtained by renormalizing the large-D limit via

$$E_3(N, Z) \approx E_\infty(N, Z + \Delta Z). \tag{VIII.2a}$$

The second version (denoted B) instead finds the renormalized charge, $Z + \delta Z$, from

$$E_\infty^{\mathrm{HF}}(N, Z + \delta Z) \equiv E_\infty(N, Z), \tag{VIII.1b}$$

and obtains the $D = 3$ approximation [144–146] (for commentary, see also [28]) by renormalizing the Hartree–Fock energy,

$$E_3(N, Z) \approx E_3^{\mathrm{HF}}(N, Z + \delta Z). \tag{VIII.2b}$$

Both versions used the same input data: $D = 3$ Hartree–Fock results [60–63] plus the large-D limit approximation derived in analytical form by Loeser for ground state N-electron atoms [68]. The latter is simplified by considering only S states and evaluating the $U + V$ minimum for a totally symmetric configuration with all electrons equivalent. Thereby, the dimensional renormalization (DR) process requires only elementary computations, little more than the solution of a quartic equation. By combining the HF approximation (which lacks correlation) with the large-D limit (which lacks exchange), both DR methods yield much better accuracy than the HF or large-D inputs.

Moreover, further improvement was obtained by augmenting the zeroth-order DR schemes indicated in Equations (8.1 and 8.2) by leading order corrections in $1/Z$ (version *A*) or $1/D$ (version *B*). In particular, when electronic configurations of the same symmetry become degenerate for $Z \to \infty$, as often occurs, it becomes important to include the zeroth-order mixing. That correction only requires diagonalizing a small matrix in a hydrogenic basis. Again, the accuracy obtained is much better than the input approximation; incorporating the leading $1/Z$ term in the DR was found to provide about 95% of the correlation energy for atoms and cations with $N = 2$–18 electrons and $Z = 2$–28. An especially instructive case for DR was the hydride ion, H^-. The large-*D* limit has a saddle point rather than a minimum, but use of a complex *D*-scaling procedure [147] enabled DR (version *B*) to obtain a good result. In another application of DR (version *A*), the dependence on Z and N of the renormalized energies for atoms and cations was examined over the range $Z, N = 2 \to 290$ [141–143] (for commentary, see also [14] and [27]). This demonstrated an excellent correspondence with the Thomas–Fermi statistical model. The DR treatment also yielded accurate results for oscillatory structure not present in the TF model and related to angular correlation of the outermost electrons [148–150]. The DR method can readily be tried using other inputs, such as the large-*D* results obtained by Sergeev in his new treatment of the Bohr model [66] or (instead of HF) the Møller–Plesset or other conventional methods.

For molecules the focus has to be on the correlation energy, which is typically comparable to or larger than the bond energy. (For example, for the F_2 molecule, the HF approximation gives better than 99.6% of the total energy, yet fails to predict that the molecule is bound.) For many-electron molecules, DR via version *A* has not been tractable but version *B* has provided a promising approach [144–146] (for commentary, see also [28]). In essence, this combines renormalized charge increments δZ_α determined for each constituent atom α with slopes, $\sigma_\alpha \equiv \partial E^{\mathrm{HF}}/\partial Z_\alpha$, computed from the *molecular* Hartree–Fock energy. The charge increments are evaluated from the *atomic* correlation energies, $\Delta E_\alpha \approx \sigma_\alpha \delta Z_\alpha$. The corresponding approximation for the correlation energy for a diatomic molecule is

$$\Delta E_{\alpha\beta} \approx \left(\sigma_\alpha + \frac{Z_\beta}{R}\right)\delta Z_\alpha + \left(\sigma_\beta + \frac{Z_\alpha}{R}\right)\delta Z_\beta + \frac{\partial E}{\partial R}\delta R. \qquad \text{(VIII.3)}$$

The Z/R terms arise from the nuclear-nuclear repulsion. The third term represents a contribution from renormalizing the internuclear distance. Its contribution is estimated [144–146] (for commentary, see also [28]) to be an order of magnitude smaller than those from renormalizing the nuclear charges; also at the equilibrium bond distance and at large R the third term vanishes. For a polyatomic molecule, the correlation energy can be obtained in the same way, just by adding analogous terms to Equation (VIII.3). Kais and coworkers [144–146] (for commentary, see also [28]) have tested this approach by determining the correlation energy at the equilibrium R for about 20 molecules, including $Be_2 \ldots F_2$; HF, LiF, BeO; H_2O, CH_2, and CH_4. Comparison with high level correlated *ab initio* calculations, MP4 and CISD(T), indicates that their DR method typically gives 70% or more of the correlation energy. This is remarkable, since beyond large-*D* results for the constituent atoms, the method requires only slight modifications of the standard Hartree–Fock algorithm. As expected, better results are obtained with input

approximations which model non-dynamical electron correlation, such as CASSCF (complete active space multiconfigurational HF) and unrestricted HF.

Further evidence for the utility of the large-D limit in evaluating electron correlation has been obtained in a study applying DR to the Hooke's Law Atom [151]. For that model, the electron–electron repulsion is Coulombic, but the electron–nucleus attraction is replaced by a harmonic oscillator potential. For a particular value of the force constant, an exact analytical solution is available [152]. Exact exchange and correlation functionals obtained for this model were used to test customary approximations employed in density functional theory [2]. Renormalization of the large-D limit gave excellent agreement with the exact results, including over 95% of the correlation energy.

As attested by the examples cited above, DR offers inviting opportunities to hybridize the large-D limit with other methods. A prime candidate is density functional theory, since the large-D limit is compatible with the large-N limit and the Kohn–Sham (KS) and HF equations are formally similar, both involving single particle orbitals. In principle the KS method can yield exact results for the energy and electron density, but in practice the accuracy is limited because the correct form for the exchange-correlation functional is not known. An alliance of D-scaling with density functional theory may provide constraints [153] useful in improving exchange-correlations functionals [151,154]. This would exploit both the utility of the large-D limit in estimating electron correlation and the ability of DFT to employ the same functionals in treating atoms and molecules. An especially appealing possibility, yet to be explored, is to introduce D-scaling into reduced density matrix mechanics. The major advances recently made in that field are reviewed in a beckoning book edited by David Mazziotti [13]. This appears to offer congenial possibilities for DR that involve treating no more than three or four electrons. Especially pertinent for DR is a chapter by Kais, devoted to relations among electron correlation, entanglement, and density matrices [155]. Again, a key aim would be to find out whether D-scaling can identify useful constraints for constructing the density matrices.

We dedicate this review to enterprising colleagues, past, present, and future, not content with brute-force computation and eager to pursue unorthodox approaches to electronic structure in the spirit of Niels Bohr.

Acknowledgements

We gratefully acknowledge the support of the Office of Naval Research (Award No. N00014-03-1-0385) and the Robert A. Welch Foundation (Grant No. A-1261).

References

[1] H. F. Schaefer, *Quantum Chemistry: The Development of Ab Initio Methods in Molecular Electronic Structure Theory* (Clarendon Press, Oxford, 1984).
[2] R. G. Parr and W. Yang, *Density-Functional Theory of Atoms and Molecules* (Clarendon Press, Oxford, 1989).
[3] C. Leichtle, W. P. Schleich, I. Sh. Averbukh, and M. Shapiro, Phys. Rev. Lett. **80**, 1418 (1998).
[4] K. A. Nelson and L. R. Williams, Phys. Rev. Lett. **58**, 745 (1987).
[5] J. P. Barnes and W. S. Warren, Phys. Rev. Lett. **85**, 856 (2000).
[6] J. L. Kinsey and B. R. Johnson, J. Phys. Chem. A **102**, 9660 (1998).

[7] K. Ohmori, Y. Sato, E. E. Nikitin, and S. A. Rice, Phys. Rev. Lett. **91**, 243003 (2003).
[8] V. S. Batista and P. Brumer, Phys. Rev. Lett. **89**, 143201 (2002).
[9] F. Sun, G. P. Glass, and R. F. Curl, Chem. Phys. Lett. **337**, 72 (2001).
[10] R. S. Berry, in *Intramolecular Dynamics*, edited by J. Jortner and B. Pullman (Reidel, Dordrecht, 1982), pp. 29–52.
[11] R. S. Berry and J. Krause, Adv. Chem. Phys. **70**, 35 (1988).
[12] J. B. Anderson, *Quantum Monte Carlo: Origins, Development, Applications* (Oxford University Press, Oxford, 2007).
[13] D. A. Mazziotti Ed., Adv. Chem. Phys. **134**, 261 (2007).
[14] D. R. Herschbach, J. S. Avery, and O. Goscinski Ed., *Dimensional Scaling in Chemical Physics* (Kluwer Academic Publishers, Dordrecht, 1992).
[15] E. Witten, Phys. Today **33** (7), 38 (1980).
[16] K. G. Wilson, Phys. Rev. Lett. **28**, 548 (1972).
[17] K. G. Wilson, Rev. Mod. Phys. **55**, 583 (1983).
[18] D. R. Herschbach, J. Chem. Phys. **84**, 838 (1986).
[19] D. Z. Goodson, M. López-Cabrera, D. R. Herschbach, and J. D. Morgan III, J. Chem. Phys. **97**, 8481 (1992).
[20] D. Z. Goodson, M. López-Cabrera, D. R. Herschbach, and J. D. Morgan III, Phys. Rev. Lett. **68**, 1992 (1992).
[21] C. T. Tsipis, V. S. Popov, D. R. Herschbach, and J. S. Avery, *New Methods in Quantum Theory* (Kluwer Academic Publishers, Dordrecht, 1996).
[22] L. G. Yaffe, Rev. Mod. Phys. **54**, 407 (1982).
[23] L. G. Yaffe, Phys. Today **36** (8), 50 (1983).
[24] D. R. Herschbach, J. Chem. Soc. Faraday Disc. **84**, 465 (1987).
[25] A. Chatterjee, Phys. Rep. **186**, 249 (1900).
[26] D. R. Herschbach, in *The Chemical Bond: Structure and Dynamics*, edited by A. Zewail (Academic Press, New York, 1992), pp. 175–222.
[27] D. R. Herschbach, Int. J. Quantum Chem. **57**, 295 (1996).
[28] J. G. Loeser and D. R. Herschbach, in *New Methods in Quantum Theory*, edited by C. T. Tsipis, V. S. Popov, D. R. Herschbach, and J. S. Avery (Kluwer Academic Publishers, Dordrecht, 1996), pp. 1–32.
[29] N. Bohr, Phil. Mag. **26**, 1 (1913).
[30] N. Bohr, Phil. Mag. **26**, 476 (1913).
[31] N. Bohr, Phil. Mag. **26**, 857 (1913).
[32] J. H. Van Vleck, Phil. Mag. **44**, 842 (1922).
[33] A. Sommerfeld, *Atomic Structure and Spectral Lines*, 3rd ed. (E.P. Dutton & Company Publishers, New York, 1923), pp. 76–78.
[34] A. A. Svidzinsky, M. O. Scully, and D. R. Herschbach, Phys. Rev. Lett. **95**, 080401 (2005).
[35] D. D. Frantz and D. R. Herschbach, Chem. Phys. **126**, 59 (1988).
[36] W. Kolos and L. Wolniewicz, J. Chem. Phys. **43**, 2429 (1965).
[37] W. Kolos and L. Wolniewicz, J. Chem. Phys. **49**, 404 (1968).
[38] C. C. J. Roothaan, Rev. Mod. Phys. **23**, 69 (1951).
[39] A. L. Parson, Smithsonian Inst. Publ., Miscel. Collections **65**, No. 11 (1915).
[40] G. N. Lewis, J. Am. Chem. Soc. **38**, 762 (1916).
[41] W. Kossel, Ann. Physik **49**, 229 (1916).
[42] M. Born, Verh. deut. Phys. Ges. **20**, 230 (1918).
[43] A. Landé, Verh. Deut. Phys. Ges. **21**, 2 (1919).
[44] A. Landé, Verh. Deut. Phys. Ges. **21**, 644 (1919).
[45] A. Landé, Verh. Deut. Phys. Ges. **21**, 653 (1919).
[46] A. Landé, Zeit. f. Physik. **2**, 83 (1920).

[47] A. Landé, Zeit. f. Physik. **2**, 380 (1920).
[48] I. Langmuir, Proc. Nat. Acad. Sci. **5**, 252 (1919).
[49] R. D. Harcourt, J. Phys. B: At. Mol. Phys. **16**, 2647 (1983).
[50] M. Gutzwiller, *Chaos in Classical and Quantum Mechanics* (Springer, Berlin, 1990).
[51] J. S. Briggs, Aust. J. Phys. **52**, 341 (1999).
[52] J. A. West, Z. D. Gaeta, and C. R. Stroud Jr, Phys. Rev. A **58**, 186 (1998).
[53] C. F. Bunge and J. A. Barrientos, Atom. Data Nucl. Data Tables **53**, 113 (1993).
[54] L. Pauling, J. Am. Chem. Soc. **53**, 1367 (1931).
[55] J. C. Slater, Phys. Rev. **37**, 481 (1931).
[56] C. A. Coulson, *Valence*, 2nd ed. (Oxford University Press, London, 1952).
[57] F. Weinhold and C. R. Landis, *Valence and Bonding: A Natural Bound and Orbital Donor–Acceptor Perspective* (Cambridge University Press, Cambridge, 2005).
[58] E. Clementi and C. Roetti, At. Data Nucl. Data Tables **14**, 177 (1974).
[59] A. D. McLean and R. S. McLean, At. Data Nucl. Data Tables **26**, 197 (1981).
[60] J. P. Desclaux, At. Data Nucl. Data Tables **12**, 311 (1973).
[61] A. Veillard and E. Clementi, J. Chem. Phys. **49**, 2415 (1968).
[62] R. D. Cowan, *The Theory of Atomic Structure and Spectra* (University of California, Berkeley, 1981), p. 203.
[63] A. C. Larson and J. T. Weber, J. Chem. Phys. **48**, 5021 (1968).
[64] N. Bohr, Phil. Mag. **26**, 492 (1913).
[65] I. Langmuir, Phys. Rev. **17**, 339 (1921).
[66] A. Sergeev, in production.
[67] B.-G. Engtert and J. Schwinger, Phys. Rev. A **32**, 47 (1985).
[68] J. G. Loeser, J. Chem. Phys. **86**, 5635 (1987).
[69] N. Bohr, in *Bohr: Collected Works*, edited by L. Rosenfeld (North-Holland Publishing Company, Amsterdam, New York, Oxford, 1981), Vol. 2, p. 153.
[70] W. Heitler and F. London, Zeit. f. Phys. **44**, 455 (1927).
[71] A. Lopez-Castillo, Phys. Rev. Lett. **77**, 4516 (1996).
[72] L. Wolniewicz and K. Dressler, J. Chem. Phys. **100**, 444 (1994).
[73] G. Theodorakopoulos, S. C. Farantos, R. J. Buenker, and S. D. Peyerimhoff, J. Phys. B: Mol. Phys. **17**, 1453 (1984).
[74] M. Aubert, N. Bessis, and G. Bessis, Phys. Rev. A **12**, 2298 (1975).
[75] R. P. Saxon, K. T. Gillen, and B. Liu, Phys. Rev. A **15**, 543 (1977).
[76] R. J. Gdanitz, Molec. Phys. **96**, 1423 (1999).
[77] K. K. Docken and J. Hinze, J. Chem. Phys. **57**, 4928 (1972).
[78] D. L. Cooper, J. Chem. Phys. **80**, 1961 (1984).
[79] I. Schmidt-Mink, W. Muller, and W. Meyer, Chem. Phys. **92**, 263 (1985).
[80] I. Hubac and M. Svrcek, J. Chem. Phys. **84**, 3260 (1986).
[81] A. Svidzinsky, S. Chin, and M. Scully, Phys. Lett. A **355**, 373 (2006).
[82] A. I. Boothroyd, W. J. Keogh, P. G. Martin, and M. R. Peterson, J. Chem. Phys. **95**, 4343 (1991).
[83] Z. Peng, S. Kristyan, A. Kuppermann, and J. S. Wright, Phys. Rev. A **52**, 1005 (1995).
[84] S. C. Wang, Phys. Rev. **31**, 579 (1928).
[85] G. Herzberg, *Molecular Spectra and Molecular Structure. I. Diatomic Molecules* (Prentice-Hall, New York, 1939).
[86] D. R. Herschbach, J. G. Loeser, and D. K. Watson, Z. Phys. D – Atoms, Molecules and Clusters **10**, 195 (1988).
[87] M. J. M. Hill, Trans. Cambridge Phil. Soc. **13**, 36 (1883).
[88] J. D. Louck, J. Mol. Spect. **4**, 285 (1960).
[89] J. D. Louck, J. Mol. Spect. **4**, 298 (1960).

[90] J. D. Louck, J. Mol. Spect. **4**, 334 (1960).
[91] G. Chen, S. A. Chin, Yu. Dou, K. T. Kapale, M. Kim, A. A. Svidzinsky, K. Urtekin, H. Xiong, and M. O. Scully, Adv. Atom. Molec. Optical Phys. **51**, 93 (2005).
[92] J. Avery, *Hyperspherical Harmonics: Applications in Quantum Theory* (Kluwer, Dordrecht, 1989).
[93] D. R. Herrick, J. Math. Phys. **16**, 289 (1975).
[94] J. Avery, D. Z. Goodson, and D. R. Herschbach, Theo. Chem. Acta **81**, 1 (1991).
[95] J. G. Loeser and D. R. Herschbach, J. Chem. Phys. **84**, 3893 (1986).
[96] D. Z. Goodson and D. R. Herschbach, J. Chem. Phys. **86**, 4997 (1987).
[97] P. du T. van der Merwe, J. Chem. Phys. **81**, 5976 (1984).
[98] P. du T. van der Merwe, J. Chem. Phys. **82**, 5293 (1985).
[99] P. du T. van der Merwe, Phys. Rev. A **34**, 3452 (1986).
[100] S. Kais and D. R. Herschbach, J. Chem. Phys. **100**, 4367 (1994).
[101] M. López-Cabrera, A. L. Tan, and J. G. Loeser, J. Phys. Chem. **97**, 2467 (1993).
[102] A. L. Tan and J. G. Loeser, in *Dimensional Scaling in Chemical Physics*, edited by D. R. Herschbach, J. S. Avery, and O. Goscinski (Kluwer Academic Publishers, Dordrecht, 1992), pp. 230–255.
[103] J. P. Tatum, Int. J. Quantum Chem. **X**, 967 (1976).
[104] C. L. Pekeris, Phys. Rev. **115**, 1216 (1959).
[105] S. Chandrasekhar and G. Herzberg, Phys. Rev. **98**, 1050 (1955).
[106] S. A. Chin, Phys. Rev. A **42**, 6991 (1990).
[107] M. Dunn and D. K. Watson, Phys. Rev. A **59**, 1109 (1999).
[108] J. M. Rost, S. M. Sung, D. R. Herschbach, and J. S. Briggs, Phys. Rev. A **46**, 2410 (1992).
[109] D. Z. Goodson and D. K. Watson, Phys. Rev. A **48**, 2668 (1993).
[110] J. C. Carzoli, M. Dunn, and D. K. Watson, Phys. Rev. A **59**, 182 (1999).
[111] R. Murawski and A. A. Svidzinsky, Phys. Rev. A **74**, 042507 (2006).
[112] P. C. Ojha and R. S. Berry, Phys. Rev. A **36**, 1575 (1987).
[113] E. Lindroth, Phys. Rev. A **49**, 4473 (1994).
[114] R. H. Garstang, Rep. Prog. Phys. **40**, 105 (1977).
[115] A. R. P. Rau, R. O. Mueller, and L. Spruch, Phys. Rev. A **11**, 1865 (1975).
[116] C. M. Bender, L. D. Mlodinov, and N. Papanicolaou, Phys. Rev. A **25**, 1305 (1982).
[117] J. R. Walkup, M. Dunn, D. K. Watson, and T. C. Germann, Phys. Rev. A **58**, 4668 (1998).
[118] A. V. Sergeev and D. Z. Goodson, Int. J. Quantum Chem. **69**, 183 (1998).
[119] A. V. Sergeev, 'Fermi-like resonances for circular Rydberg states of a hydrogen atom in a magnetic field', unpublished.
[120] T. C. Germann, J. Phys. B **28**, L531 (1995).
[121] G. Wunner, M. Kost, and H. Ruder, Phys. Rev. A **33**, 1444 (1986).
[122] M. Gravila, in *Atoms and Molecules in Superintense Laser Fields*, edited by M. Gravila (Academic, New York, 1992), p. 435.
[123] J. H. Eberly and K. C. Kulander, Science **262**, 1229 (1993).
[124] E. van Duijn, M. Gavrila, and H. G. Muller, Phys. Rev. Lett. **77**, 3759 (1996).
[125] Q. Wei, S. Kais, and N. Moiseyev, J. Chem. Phys. **124**, 201108 (2006).
[126] N. J. van Druten, R. C. Constantinescu, J. M. Schins, H. Nieuwenhuize, and H. G. Muller, Phys. Rev. A **55**, 622 (1997).
[127] N. Moiseyev and L. S. Cederbaum, J. Phys. B **32**, L279 (1999).
[128] Q. Wei, S. Kais, and D. Herschbach, J. Chem. Phys. **127**, 094301 (2007).
[129] P. Coffey, *Cathedrals of Science: Personalities and Rivalries that Made Modern Chemisty* (Oxford University Press, Oxford, 2008).
[130] R. Millikan, J. Chem. Soc. **125**, 1405 (1924).
[131] J. G. Loeser, J. H. Summerfield, A. L. Tan, and Z. Zheng, J. Chem. Phys. **100**, 5036 (1994).

[132] R. P. Feynman, R. B. Leighton, and M. Sands, *The Feynman Lectures on Physics* (Addison-Wesley, Reading, MA, 1965), Vol. III, pp. 2–6.
[133] S. Kais, J. D. III Morgan, and D. R. Herschbach, J. Chem. Phys. **95**, 9028 (1991).
[134] S. Kais, D. D. Frantz, and D. R. Herschbach, Chem. Phys. **161**, 393 (1992).
[135] D. Z. Goodson, in *New Methods in Quantum Theory*, edited by C. T. Tsipis, V. S. Popov, D. R. Herschbach, and J. S. Avery (Kluwer Academic Publishers, Dordrecht, 1996), pp. 71–82, references cited therein.
[136] P. Serra and S. Kais, Phys. Rev. Lett. **77**, 466 (1996).
[137] P. Serra and S. Kais, Int. Rev. Phys. Chem. **19**, 97 (2000).
[138] Q. Shih, S. Kais, F. Remacle, and R. D. Levine, Chem. Phys. Chem. **2**, 434 (2001).
[139] S. Kais and P. Serra, Adv. Chem. Phys. **125**, 1 (2003).
[140] J. G. Loeser, in *New Methods in Quantum Theory*, edited by C. T. Tsipis, V. S. Popov, D. R. Herschbach, and J. S. Avery (Kluwer Academic Publishers, Dordrecht, 1996), pp. 33–54.
[141] S. Kais, S. M. Sung, and D. R. Herschbach, J. Chem. Phys. **99**, 5184 (1993).
[142] S. Kais, S. M. Sung, and D. R. Herschbach, Int. J. Quantum Chem. **49**, 657 (1994).
[143] S. Kais and D. R. Herschbach, J. Chem. Phys. **100**, 4367 (1994).
[144] S. Kais and R. Bleil, J. Chem. Phys. **102**, 7472 (1995).
[145] R. Bleil, A. Faliks, M. Miletic, and S. Kais, J. Chem. Phys. **103**, 6529 (1995).
[146] S. Kais and R. Bleil, in *New Methods in Quantum Theory*, edited by C. T. Tsipis, V. S. Popov, D. R. Herschbach, and J. S. Avery (Kluwer Academic Publishers, Dordrecht, 1996), pp. 55–70.
[147] J. M. Rost, J. Phys. Chem. **97**, 2461 (1993).
[148] B. G. Englert and J. Schwinger, Phys. Rev. A **32**, 26 (1985).
[149] B. G. Englert and J. Schwinger, Phys. Rev. A **32**, 36 (1985).
[150] B. G. Englert and J. Schwinger, Phys. Rev. A **32**, 47 (1985).
[151] S. Kais, D. R. Herschbach, N. C. Handy, C. W. Murray, and G. J. Laming, J. Chem. Phys. **99**, 417 (1993).
[152] S. Kais, R. D. Levine, and D. R. Herschbach, J. Chem. Phys. **91**, 7791 (1989).
[153] M. Levy and J. P. Perdew, Int. J. Quantum Chem. **49**, 539 (1994).
[154] S. M. Valone, Int. J. Quantum Chem. **49**, 591 (1994).
[155] S. Kais, in *Reduced-Density-Matrix Mechanics, with Applications to Many-Electron Atoms and Molecules*, edited by D. A. Mazziotti, Adv. Chem. Phys. **134**, 493 (2007).